

WP 10 Deliverable No. 10.3 – D63

First Report on results of the X-ray optics measured at

PANTER

V. Burwitz, M. Bradshaw, P. Friedrich, G.Hartner, A. Langmeier, T. Müller, S. Rukdee, T. Schmidt
MPE

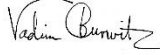
Project acronym:
AHEAD2020

Project Title:
Integrated Activities for the High Energy Astrophysics Domain

Grant Agreement No: **871158**

**This deliverable is part of a project that has received funding from the European Union's
Horizon 2020 research and innovation programme**

Start date of the project:
2020-03-02

| Version | Revision Date | Prepared by | Review and approval |
|---------|---------------|-------------|---|
| 1.0 | 07.11.2022 | V. Burwitz |  |
| | | | |
| | | | |
| | | | |
| | | | |

| Distribution List | Date | Version |
|-------------------|------------|---------|
| Lorenzo Natalucci | 07.11.2022 | 1.0 |
| | | |
| | | |
| | | |
| | | |
| | | |

Contents

| | |
|--|----|
| Contents | 5 |
| Table of Figures | 6 |
| Table of Tables..... | 9 |
| List of Acronyms | 10 |
| 1 Introduction..... | 12 |
| 2 Overview of measurement campaigns..... | 13 |
| 3 Overview of Missions | 14 |
| 3.1 SVOM..... | 14 |
| 3.2 Einstein Probe..... | 15 |
| 3.3 ATHENA | 16 |
| The ATHENA Optics | 17 |
| 4 Results obtained at PANTER..... | 18 |
| 4.1 SVOM-MXT Optic Testing at PANTER..... | 18 |
| 4.2 SVOM-MXT: Telescope Testing at PANTER | 20 |
| 4.3 Einstein Probe: FXT Optic Testing at PANTER..... | 23 |
| 4.3.1 MEASUREMENT METHODS | 23 |
| 4.3.2 RESULTS | 27 |
| 4.3.3 DISCUSSION EP-FXT | 32 |
| 4.4 Einstein Probe: WXT Optic Testing at PANTER..... | 33 |
| 4.4.1 SETUP & ALIGNMENT | 33 |
| 4.4.2 MEASUREMENT METHODS | 34 |
| 4.4.3 RESULTS | 36 |
| 4.4.4 DISCUSSION EP-WXT..... | 41 |
| 4.5 ATHENA: Testing a SPO Calibration Reference Mandrel..... | 42 |
| 4.5.1 THE OPTIC | 42 |
| 4.5.2 TEST METHODOLOGY | 43 |
| 4.5.3 Measurements..... | 45 |
| 4.5.4 RESULTS | 45 |
| 4.5.5 SUMMARY | 48 |
| 4.6 Other Campaigns at PANTER..... | 49 |
| 4.6.1 X-ray Optics for BEaTRiX..... | 49 |

| | | |
|-------|--------------------------------------|----|
| 4.6.2 | Lobster-eye and K-P Baez optics..... | 49 |
| 5 | Summary..... | 50 |
| | Bibliography..... | 51 |

Table of Figures

| | | |
|-----------|---|----|
| Figure 1 | Overview of the Space Variable Objects Monitor (SVOM). The SVOM-MXT X-ray telescope that was tested at PANTER is located at the top right of the image. | 14 |
| Figure 2 | Overview of the Einstein Probe observatory with the twelve WXT and two FXT telescopes onboard. | 15 |
| Figure 3 | Overview of the ATHENA observatory with the its $f = 12$ m focal length and 2.6 m diameter mirror assembly facing us together with the SIM science instrument module at the rear end that houses the WFI wide field imager and the XIFU calorimeter. | 16 |
| Figure 4 | (left) a mid-radius ($r = 737$ mm, $f = 120$ mm) silicon pore optic made up of to XOUs (right) the ATHENA 2.6 m diameter mirror assembly with place for mounting the 600 SPOs attached spacecraft hexapod that allows switching between the WFI and XIFU instruments..... | 17 |
| Figure 5 | (left) The SVOM-MXT-MOP flight Model (FM) optics in the PANTER vacuum chamber, view from the source toward the detector is shown (right) the coordinate. | 19 |
| Figure 6 | Measurements of the MXT-MOP-FM at Al-K (1.5 keV): (top left) a grid of 3×3 TRoPIC images combined to study the cross arms of the PSF in detail, (top right) a so-called focal plane map obtained to study variation of the PSF and efficiency of the optic on-axis as well as for a grid of off-axis angles. (bottom) the PSF as a function of energy is shown from left to right C-K, O-K, Cu-L, Al-K, Ag-L, Ti-K, Fe-K, Cu-K. | 19 |
| Figure 7 | The PANTER thermal shroud and its MLI covering are visible above the MXT-FM. The MXT-FM model in the chamber, (left) with the MOP cover removed, prior to closing the chamber door and pumping down. Photo is taken looking from the direction of the X-ray source. (right) The detector end of the MXT inside the chamber, shortly before closing the chamber and pumping down. The PANTER thermal shroud and its MLI covering are visible above the MXT-FM. Photo is taken facing the X-ray source..... | 21 |
| Figure 8 | (top) Diagram showing the position of the Telescope, and the measurement position $d7 = 10282 \pm 2$ mm in the chamber. (bottom) shows the coordinate system used during the telescope tests..... | 21 |
| Figure 9 | Measurement strategy showing the positions chosen for the location of the PSF on the detector with the corresponding pitch and yaw angles to which the telescope has to be oriented to.. | 22 |
| Figure 10 | This plot shows the effective area of the SVOM-MXT-FM telescope as measured in PANTER during the performance tests: in green the effective area measurements at the characteristic lines of the X-ray source target elements available at PANTER, in red the continuum flux measurements and in black the effective area model prediction. | 22 |
| Figure 11 | The Burkert test result at Al-K. Clockwise from top with angles relative to laser alignment: positive pitch (+19.0 arcmin), negative yaw (-20.1 arcmin), negative pitch (-16.0 arcmin), positive yaw (+15.5 arcmin). The central image is the resulting on-axis PSF, in preliminary best focus. | 23 |

| | |
|--|----|
| Figure 12 Sectors illuminated in almost parallel beam by the “Glücksrad” one after the other; left: outer sectors for shells 1 to 18 with 22.5 ° azimuthal width, right: inner sectors for shells 19 to 54 with 45 ° azimuthal width; the support structure of the “Glücksrad” blocks the outer sector 11 fully and half of the inner sector 6 (shaded area). | 25 |
| Figure 13 The two grids for focal plan mapping in a 60 arcmin × 60 arcmin square. | 27 |
| Figure 14 The compilation results of the focus search and the hyperbola fit to determine the best focus position, the smallest PSF (minimum of HEW), for the QM at Al-K. | 28 |
| Figure 15 The compilation of images of the deep PSF of the QM at Al-K with PIXI intra- (left), and extra-focal (right). | 29 |
| Figure 16 Compilation of intra-focal images for different sectors of the QM MA selected by different positions of the “Glücksrad” at different energies: (Top row) IEbc, mEbc, Al-K, Ag-L (Bottom row) Ti-K, Fe-K, Cu-K respectively, for the qualification model. Sector 11 is fully obscured by the support arm of the “Glücksrad” | 29 |
| Figure 17 The effective area measurements of the QM MA overlaid with the theoretical model. The summary of effective area at low energy band continuum at different sectors are shown with different color: dark blue for inner sectors, light blue for the outer sectors and red for the total mirror. The small triangles are the measured data points for the energies Al-K, W-M and Ag-L. | 30 |
| Figure 18 Composed focal plane mapping at different energies (left to right) Al-K, Ag-L, Ti-K, Fe-K, Cu-K respectively for the QM. | 31 |
| Figure 19 Vignetting curves for all five energies: Al-K, Ag-L, Ti-K, Fe-K, and Cu-K in comparison for the QM. | 31 |
| Figure 20 The PANTER coordinate system. The EP-WXT is mounted on the manipulator. The different sectors are labeled. | 33 |
| Figure 21 The WXT installed inside the PANTER chamber. (Left) The MPO mounted in the chamber, with the alignment laser centred on the MPO and the TRoPIC camera visible in the background (photo taken facing Pantolsky-Küche. (Right) The back side of the MPO inside the chamber. | 34 |
| Figure 22 The first image of alignment under X-ray (right) compare to the simulated result (left) | 34 |
| Figure 23 The focus search at Cu-L (PANTER analysis) for all sectors, with the calculated FWHM plotted against the corresponding axis position. The blue cross indicates the fitted best focus position. The green diamonds are the FWHM in x and the red triangles are the ones in y, from a simple Gaussian fit. | 37 |
| Figure 24 Compilation image of the on-axis in focus, extended (3x3) mosaic for each of the four sectors at Cu-L, from left to right are the PSF from sector 1 to 4 respectively. | 37 |
| Figure 25 Compilation image of the on-axis in focus, extended (3x3) mosaic of the two sectors at Ti-K for section 1 (left) and sector 2 (right). | 38 |
| Figure 26 Compilation image of the on-axis in focus, extended (3x3) mosaic of the two sectors at vIEbc for section 1 (left) and sector 2 (right). | 38 |
| Figure 27 Compilation of PSF exposures for the focal plane mapping at all sectors: sector 1 (top left), sector 2 (top right), sector 3 (bottom left), sector 4 (bottom right) in horizontal, vertical and diagonal direction Cu-L. | 39 |
| Figure 28 Compilation of PSF exposures for the focal plane mapping at sector 2 in horizontal (yaw), vertical (pitch) direction at C-K, Cu-L and Ti-K for the off-axis angle from -150 arcmin to 150 arcmin. | 40 |

| | |
|--|----|
| Figure 29 The effective area of single reflection, double reflection, and direct beam at ν Ebc (VLE) and ν Ebc(LE) for all 4 sectors (S1, S2, S3, S4) in comparison with different models..... | 41 |
| Figure 30 Photograph of the XOU-0055 mandrel optic, showing (a) the parabolic M48 mandrel and (b) the hyperbolic M50 mandrel (Photo credit: cosine measurement systems)..... | 43 |
| Figure 31 (a) The XOU-0055 mounted inside the PANTER chamber attached to a hexapod, to enable fine adjustment of the optic under vacuum. The moveable mask used to illuminate either the full optic or a chosen section of the optic is also shown. The MLI between the optic and the hexapod protects the optic from the heat produced by the hexapod motors. (b) The optic in its holding structure at the PANTER facility, showing the nomenclature for the measurements of the optic during this campaign. (Credit: MPE) | 44 |
| Figure 32 The best focus PSF image for (a) the full optic with the 100% mask, and (b) the bottom ~30% of the optic with the 48% mask. The corresponding HEW values are written on the appropriate image. (Credit: MPE)..... | 46 |
| Figure 33 The HEW at each position of the azimuthal scan, aligning the 4% mask in front of the optic, starting at the ‘top’ of the optic, and measuring 24 separate positions (each one a separate exposure) to the ‘bottom’ of the optic. (Credit: MPE) | 47 |
| Figure 34 Intra-focal 220 mm (a) full image and (b) x4 zoomed image of XOU-0055, at the best full optic focus position, taken at Al-K using the 100% mask..... | 47 |
| Figure 35 Extra-focal 250 mm (a) full image and (b) x4 zoomed image of XOU-0055, at the best full optic focus position, taken at Al-K using the 100% mask..... | 48 |
| Figure 36 Extra-focal 340 mm (a) full image and (b) x4 zoomed image of XOU-0055, at the best full optic focus position, taken at Al-K using the 100% mask..... | 48 |
| Figure 37 (left) the BEaTriX paraboloidal mirror mounted in PANTER, viewed from the detectors side. (center) Best focus measured with PIXI at 1.49 keV in parallel setup, before coating, HEW = 3.1 arcsec. (right) Same as previous image but after coating, HEW = 2.8 arcsec. | 49 |
| Figure 38 Large KB module at the PANTER facility. (left) view from X-ray source, (right) the side view... | 49 |

Table of Tables

| | |
|--|----|
| Table 1 List of campaigns performed at PANTER in part supported by the AHEAD2020 JRA X-ray optics | 13 |
| Table 2 Requirements for orbit and derived requirements for PANTER X-ray test of the FXT | 16 |
| Table 3 Overview of the SVOM-MXT optics tests performed and planned at the PANTER X-ray test facility, high- lighted in green are the AHEAD, and in blue the AHEAD 2020 activities. | 18 |
| Table 4 Overview of the SVOM-MXT telescope tests performed at the PANTER X-ray test facility. High- lighted in blue are the AHEAD 2020 activities | 20 |
| Table 5 Summary of the calibration measurements for the FXT QM and FM | 32 |
| Table 6 Summary of the focus search result and analysis at Cu-L | 36 |
| Table 7 Specifications of the XOU-0055 optic, comprising two mandrels to create one silicon reflective 'layer' | 43 |
| Table 8 The HEW values of the optic for each measurement set, showing the mask used and the section of the optic imaged..... | 46 |

List of Acronyms

| | |
|---------|---|
| ACC | post ACCEptance X-ray test |
| AHEAD | integrated Activities for the High Energy Astrophysics Domain |
| ATHENA | Advanced Telescope for High-ENERgy Astrophysics |
| BAF | post BAFFle test |
| BB | Bread Board |
| BEaTriX | Beam Expander Testing X-ray |
| CAL | post CALibration X-ray test |
| CAS | Chinese academy of science |
| CCD | Charge Coupled Device |
| CEA | Commissariat à l'Énergie Atomique et aux énergies alternatives |
| CXO | Chandra X-ray Observatory (NASA) |
| CMOS | Complementary Metal Oxide Semiconductor |
| CNES | Centre National d'Etude Spatiales (French Space Agency) |
| CNSA | China National Space Administration |
| DLR | Deutsche Luft und Raumfahrt (German Space Agency) |
| EP | Einstein Probe |
| eROSITA | extended ROentgen Survey with an Imaging Telescope Array |
| ESA | European Space Agency |
| FM | Flight Model |
| FS | Flight Spare |
| FXT | Follow up X-ray Telescope |
| IHEP | Institute for High Energy Physics in Beijing |
| IRFU | Institute of Research into the Fundamental Laws of the Universe |
| IJC-Lab | Irène Joliot-Curie Laboratoire de physique des 2 infinis |
| HEW | Half Energy Width |
| MA | Mirror Assembly |
| MOP | MXT OPTical assembly |
| MPE | Max Planck institute for Extraterrestrial physics |
| MPO | Micro Pore Optic |

| | |
|------------|---|
| MXT | Microchannel X-ray Telescope |
| NASA | National Aeronautics and Space Administration |
| PANTER | X-ray test facility of the high energy group at MPE |
| PSF | Point spread Function |
| QM | Qualification Model |
| ROSAT | ROentgenSATellit |
| Roskosmos | Russian Space Agency |
| SDD | Silicon Drift Detector |
| SIM | Science Instrument Module |
| SPO | Silicon Pore Optic |
| STM | Structural Test Model |
| SVOM | Space Variable Objects Monitor |
| SWIFT | Neil Gehrels Swift Observatory (NASA) |
| UoL | University of Leicester |
| VIB | Post vibration X-ray test |
| WFI | Wide Fiel Imager |
| WXT | Wide field X-ray Telescope |
| XMM-Newton | X-ray Multi-Mirror observatory (ESA) |
| XIFU | X-ray Integral Field Unit |
| XOU | Silicon pore optics X-ray Optical Unit |

1 Introduction

The PANTER X-ray test facility of the high energy group of the Max Planck Institute for Extraterrestrial Physics (MPE) was setup to help with the development, testing and calibration of the X-ray optic and detector for the ROSAT mission over 40 years ago. Since then the facility has been involved in the testing of optics, gratings, detectors as well as complete X-ray telescopes for many different missions. The currently active X-ray observatories which had components tested at PANTER are XMM-Newton (ESA), Chandra (NASA), SWIFT (NASA), eROSITA (DLR) on Spektr-RG (Roskosmos). Upcoming missions are SVOM (CNES/CAS), and Einstein Probe (CAS/ESA/MPE). And developments for future missions such as ATHENA, Arcus and other ESA M-Class, NASA MIDEX and probe missions are ongoing with optics and detectors being tested at PANTER.

The PANTER X-ray test facility is located in Neuried, to the south west of Munich. It consists of a 120 m long 1 m diameter vacuum beam line that is attached to a large vacuum chamber 12 m long and 3.5 m diameter. At the beginning of the 1 m tube a multi-target electron impact beam X-ray source is located. The source can illuminate optics with a diameter of up to 1 m in the large vacuum test chamber. The X-rays focused by the optics are measured with detectors that are also inside the vacuum chamber. Both the optics and detectors are mounted on translation and rotary/tilt stages. This freedom of movement for the optics and detectors makes it possible to test large variety of different optics and gratings in the facility.

In this document the work, which is in part supported by the AHEAD 2020, done at the PANTER X-ray test facility on testing, characterising, and calibrating X-ray optics for approved and potential future missions during the period March 2020 to Jan 2022 is summarised. A description of the PANTER test timeline, the X-ray missions SVOM, Einstein Probe and ATHENA for which the optics are being tested. Here the key results obtained during the measurement selected campaigns are presented.

In Section 2 the campaigns performed are summarised. In Section 3 an overview of the missions for which optics are being tested is given. In Section 4 the measurements at PANTER are described and results obtained presented and discussed. All the work done at PANTER supported in part by the AHEAD2020 grant is summarized in Section 5.

2 Overview of measurement campaigns

Despite Covid a really large number of test campaigns were performed at PANTER these are summarised in Table 1.

Table 1 List of campaigns performed at PANTER in part supported by the AHEAD2020 JRA X-ray optics

| Dates | Project | |
|----------|--------------------|---|
| 2020 Mar | ATHENA | XOU-0055 mandrel characterization |
| 2020 Mar | PANTER | X-ray beam spectral characterization |
| 2020 Apr | ATHENA | MM-0036 particulate contamination |
| 2020 Apr | Einstein Probe | FXT STM MA post vibration shock |
| 2020 Apr | PANTER | X-ray beam spatial characterization |
| 2020 Apr | PANTER | TRoPIC thermal investigation |
| 2020 May | Einstein Probe | FXT STM MA post thermal |
| 2020 May | Optics Development | Tongji inner layer |
| 2020 Jun | PANTER | Test zone plate |
| 2020 Jun | Optics Development | OAB uncoated drum |
| 2020 Jul | ATHENA | MM-0036 XOU-0077 post contamination 1000ppm |
| 2020 Aug | Optics Development | OAB coated drum |
| 2020 Oct | PANTER | thermal test |
| 2020 Dec | ATHENA | MM-0036 XOU-0077 post contamination 2000ppm |
| 2021 Jan | SVOM | MXT-MOP-FM |
| 2021 Feb | Optics Development | HA-MPE lobster-eye |
| 2021 Mar | Optics Development | HA-MPE lobster-eye-II |
| 2021 Apr | Einstein Probe | WXT-QM |
| 2021 May | BEaTriX | uncoated parabola |
| 2021 May | EP | FXT-QM-MM-ACC |
| 2021 Jun | BEaTriX | coated parabola |
| 2021 Jun | Einstein Probe | FXT-QM-MA-BAF |
| 2021 Jul | Einstein Probe | FXT-QM-MA-VIB |
| 2021 Aug | Einstein Probe | FXT-QM-MA-CAL |
| 2021 Sep | Optics Development | Arcus FLAT |
| 2021 Oct | SVOM | MXT-TEL-FM |
| 2021 Nov | Optics Development | Rigaku KP-Baez 6.0m |
| 2021 Nov | PANTER | SDD Characterisation |
| 2022 Jan | Einstein Probe | FXT-FM-MM-ACC |

3 Overview of Missions

3.1 SVOM

The China National Space Administration (CNSA), Chinese Academy of Sciences (CAS) and the French Space Agency (CNES) are developing the small X-ray telescope Space Variable Objects Monitor (SVOM) [1] satellite to be launched end of 2023. The mission has instruments onboard to detect gamma-ray bursts and localize them. The four main instruments are ECLAIRs: a wide field coded mask camera, GRM: a gamma-ray non-imaging spectrometer, MXT: a Microchannel X-ray Telescope, and a Visible Telescope. The mission also has a ground segment of optical follow up telescopes. See the overview in Figure 1.

The onboard Microchannel X-ray Telescope (MXT) [2] is a development led by CNES in collaboration with CEA-Saclay/IRfU, the University of Leicester, the Max Planck Institute for Extraterrestrial Physics (MPE) in Munich, and the IJC-Lab in Orsay. The SVOM-MXT, an X-ray telescope sensitive in the 0.2–10 keV energy range, is a compact (focal length ~ 1.15 m) and light (< 42 kg) instrument. The ultra-lightweight MXT Optical assembly (MOP) is a structure holding an array of 5×5 Micro Pore Optics (MPOs) following a “lobster eye” optical design [3]. Each MPO is 40 mm a side and has a thickness of 1.2 mm and 2.4 mm for the outer and inner plates respectively. Each MPO is made up of about 1000×1000 iridium coated channels (size of a single channel $40 \mu\text{m} \times 40 \mu\text{m}$) that focus the X-rays onto a low-noise pnCDD X-ray detector [4, 5]. The field of view of the telescope is approximately 57 arcmin a side with a collecting area of about 35 cm^2 at Al-K (1.5 keV).

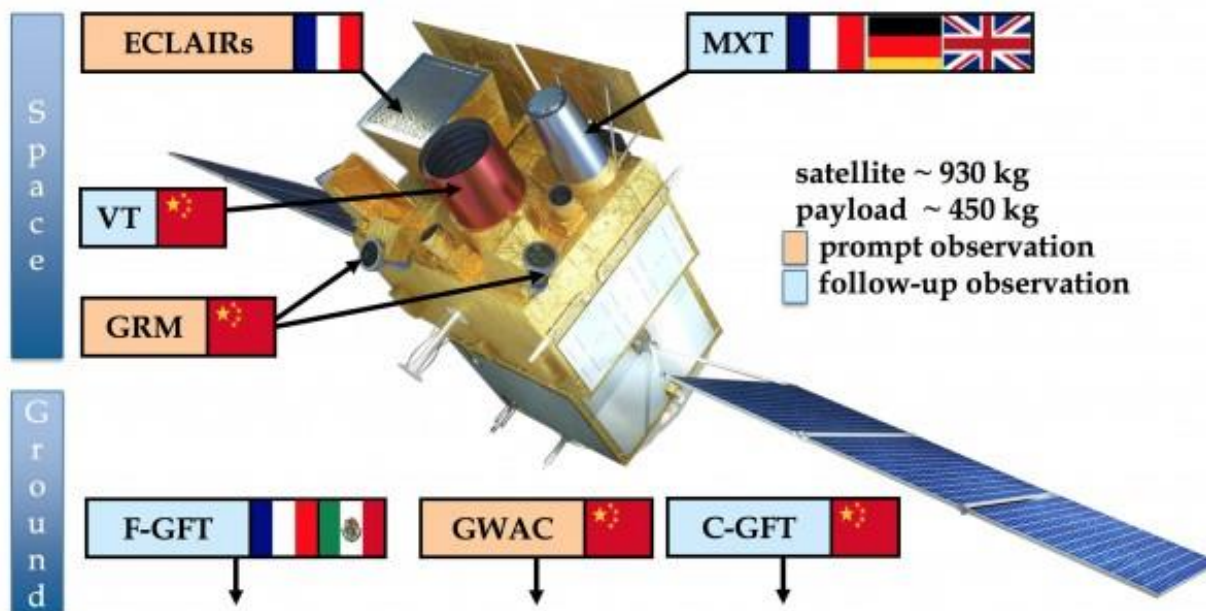


Figure 1 Overview of the Space Variable Objects Monitor (SVOM). The SVOM-MXT X-ray telescope that was tested at PANTER is located at the top right of the image.

For the last 6 years, the PANTER X-ray test facility has been involved in the development and testing of the MPO mirrors that are used in the SVOM-MXT telescope. The work on the specific 1.15 m focal length MPOs for the SVOM Mission has been ongoing since 2016. With the X-ray source at a distance of >120 m from the test optic, the PANTER beamline allows the testing with a slightly divergent beam. For the SVOM-MXT optics tests the PANTER detectors were used whilst for the telescope tests the MXT detectors were used.

3.2 Einstein Probe

The Einstein Probe (EP) [6] is a dedicated mission for time-domain high-energy astrophysics led by the Chinese Academy of Sciences (CAS) due to launch in 2023. The primary goals of the mission are to discover high-energy transients, to monitor variable objects and to search for X-ray sources associated with gravitational-wave events. The instruments on board consist of 1) the Wide-Field X-ray Telescope (WXT) [7] providing a 3,600 square degrees field of view within the energy range of 0.5-4 keV [8] and 2) the Follow-Up X-ray Telescope (FXT) [9] for the energy range 0.3-10 keV high resolution follow-up observations.



Figure 2 Overview of the Einstein Probe observatory with the twelve WXT and two FXT telescopes onboard.

The Einstein Probe follow-up telescope [9] (FXT) is the European contribution, funded by the European Space Agency (ESA), accomplished by Media Lario S.r.l., Italy, and the Max Planck Institute for Extraterrestrial Physics (MPE). The FXT is an eROSITA-like Wolter-I-type telescope [10], consisting of 54 gold-coated nickel X-ray mirror shells [11] mounted inside a case with an interface to the telescope structure, where the mirror shells are glued into a spoke wheel ('spider'). After an acceptance test with X-rays, the X-ray baffle (XRB) was precisely aligned and mounted to the mirror module. Thereafter, it is referred to as a mirror assembly (MA). The main goal of the final X-ray test and calibration is to evaluate the optic performance in terms of angular resolution (PSF images) and effective area as a function of energy of the MA. The test requirements for the FXT are described in Table 2.

Table 2 Requirements for orbit and derived requirements for PANTER X-ray test of the FXT

| | Orbit | Derived for PANTER |
|---------------------|-----------------------|--------------------------|
| HEW Al-K (1.49 keV) | 22" | 22" |
| Eff. Area Al-K | > 350 cm ² | > 348.2 cm ² |
| Eff. Area Cu-K | > 20 cm ² | > 18.7 cm ² |
| Micro-roughness | < 0.5 nm | Scattering Cu-K < 15.7 % |
| Focal length | 1600 ± mm | 1600 ± 2 mm\$ |

The WXT is a lobster eye type X-ray telescope consisting of 12 identical modules of 6x6 micro pore optics (MPOs). Each MPO is 2.5 mm thick and made from lead glass, with iridium coating and an aluminium film on the front. This optic has a focal length of 375 mm and a 3,600 square degrees field of view with a goal of 5 arcmin resolution. The focus point of each optic sector is aligned to its corresponding CMOS detector. The MPOs are individually aligned on the frame using screws at the rear of the frame and held in place with epoxy. Each MPO is held on the frame using an MPO enforcement pad and then secured using GD-414c silicone glue with small areas close to the MPOs filled with 703 silicone glue. [12] The main requirement for testing the qualification model (QM) of this optic is to understand the effective area of the module and the linearity of the off-axis response.

3.3 ATHENA

The European Space Agency ATHENA mission is an x-ray observatory that will study the formation of galaxy clusters and the growth of black holes. Due for launch in early 2030s, with adoption planned for 2022, ATHENA will use 600 silicon pore optic mirror modules to create a 2.6 m diameter X-ray mirror.

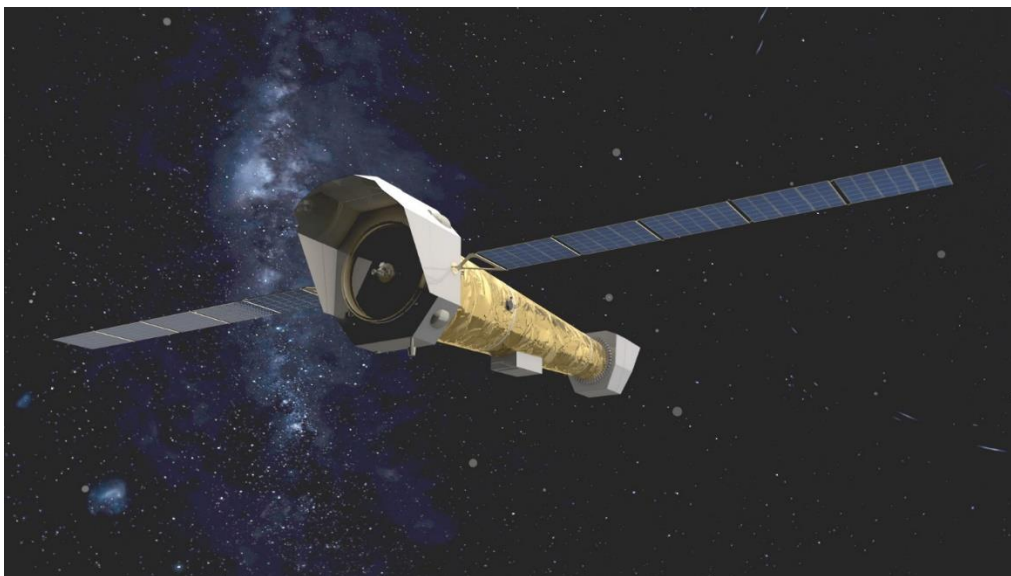


Figure 3 Overview of the ATHENA observatory with the its $f = 12$ m focal length and 2.6 m diameter mirror assembly facing us together with the SIM science instrument module at the rear end that houses the WFI wide field imager and the XIFU calorimeter.

ATHENA – the Advanced Telescope for High-Energy Astrophysics – is an x-ray telescope led by the European Space Agency. Due to launch in mid 2030s, it will map hot gas structures in clusters and groups of galaxies, study the shape and growth of supermassive black holes, and explore high-energy astrophysical events such as supernova explosions [13]. To achieve this, ATHENA will carry two instruments: the X-ray Integral Field Unit (XIFU) [14], an X-ray spectrometer, and the Wide Field Imager (WFI) [15], a silicon-based detector. A single telescope, based on silicon pore optic (SPO) technology, will focus the X-rays onto one of the two instruments at any given time using an “instrument switching” mechanism [16]. ATHENA will observe in the energy range of 0.2 – 12.0 keV.

The ATHENA Optics

The telescope of ATHENA has the following specifications [16]:

- a focal length of 12 m,
- a half energy width (HEW) angular resolution of 5 arcseconds at 1 keV, and
- an effective area of ≥ 1.4 m² at 1 keV, and ≥ 0.25 m² at 6 keV.

The optics for the ATHENA telescope are silicon pore mirror modules SPOs (Figure 4 left), an X-ray optic technology designed by cosine measurement systems specifically for the ATHENA mission [17].

To create the optics, 35 ribbed silicon mirror “plates” are stacked together, each rib creating a pore once the plates are stacked. A co-aligned pair of such stacks, representing the primary parabolic and the secondary hyperbolic mirror in a Wolter-I-type optic, creates an ‘X-ray optical unit’ (XOU). Two XOUs make up one mirror module (MM), which focuses incoming X-rays into an image. The ATHENA telescope will comprise nearly 700 mirror modules (Figure 4 right).

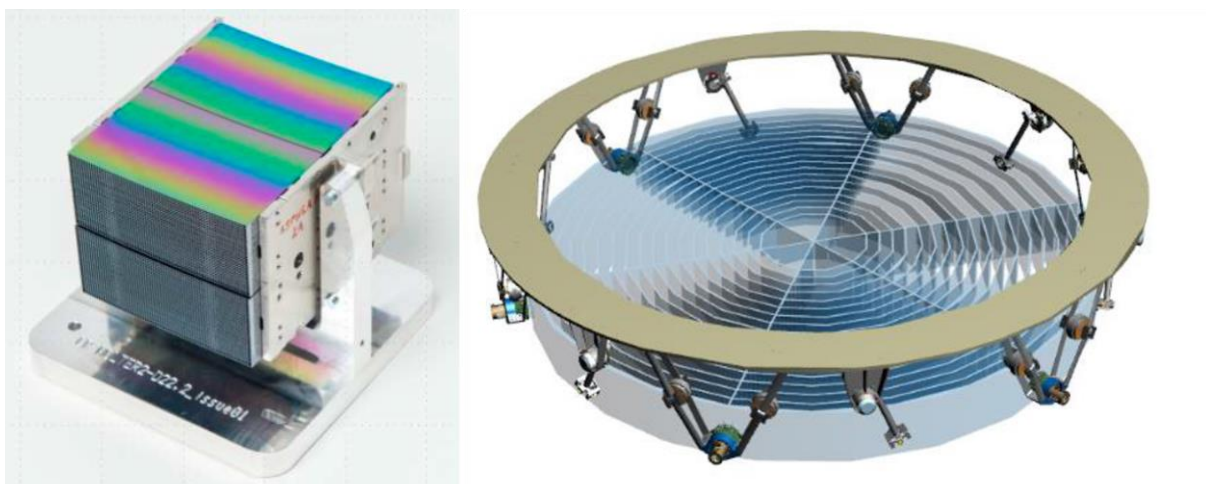


Figure 4 (left) a mid-radius ($r = 737$ mm, $f = 120$ mm) silicon pore optic made up of two XOUs (right) the ATHENA 2.6 m diameter mirror assembly with place for mounting the 600 SPOs attached spacecraft hexapod that allows switching between the WFI and XIFU instruments.

4 Results obtained at PANTER

4.1 SVOM-MXT Optic Testing at PANTER

The performance of the SVOM-MXT optics (MOP) Flight Model (FM) was characterized in Jan./Feb. 2021. Table 3 lists all optics test campaigns. A photo the MOP flight model in the PANTER vacuum chamber are shown in Figure 5.

At PANTER, it is possible to characterize optics in great detail. The multi-target X-ray source allows measurements be made at many different energies from B-K at 0.18 keV through Al-K at 1.5 keV all way up to Ge-K β at 11 keV. This covers the range at which the MXT telescope will work and the measurements were done at most of these available energies. A clean energy selection is possible as the TRoPIC pnCCD detector available at PANTER is operated in single photon counting allowing for a good determination of the photon energy.

The optics test at PANTER consisted of:

- Optical laser pre-alignment before pump down
- X-ray pitch and yaw alignment
- Focus search scans
- Deep PSF measurements (see Figure 6 top, left and bottom)
 - to study the cross arms of the PSF in detail
- Focal plane scans covering a grid of pitch and yaw angles (see Figure 6 top, right)
 - to study the dependence of the PSF and effective area on the off-axis angle.

The focus scans were done at C-K, Al-K, and Ti-K. The deep PSF and Focal plane scans were executed in several different energies from C-K to Cu-K. In addition, continuum flux measurements were performed to consolidate the shape of the effective area curves between the single energy measurements.

Table 3 Overview of the SVOM-MXT optics tests performed and planned at the PANTER X-ray test facility, high- lighted in green are the AHEAD, and in blue the AHEAD 2020 activities.

| Optic Tests | Date | Optic | Type of tests [reference] |
|--------------------------|-------------------------|-----------------|--------------------------------|
| Bread Board (BB) | Jul. 11 – Jul. 15, 2016 | 7 MPOs | Testing individual MPOs [8] |
| Qualification Model (QM) | Jul. 10 – Jul. 26, 2019 | Fully populated | Calibration (test run) [12] |
| Flight Model (FM) | Jan. 11 – Feb. 04, 2021 | Fully populated | Calibration (final) [in Prep.] |
| Flight Spare (FS) | May 02 – May14, 2022 | Fully populated | Planned measurement |

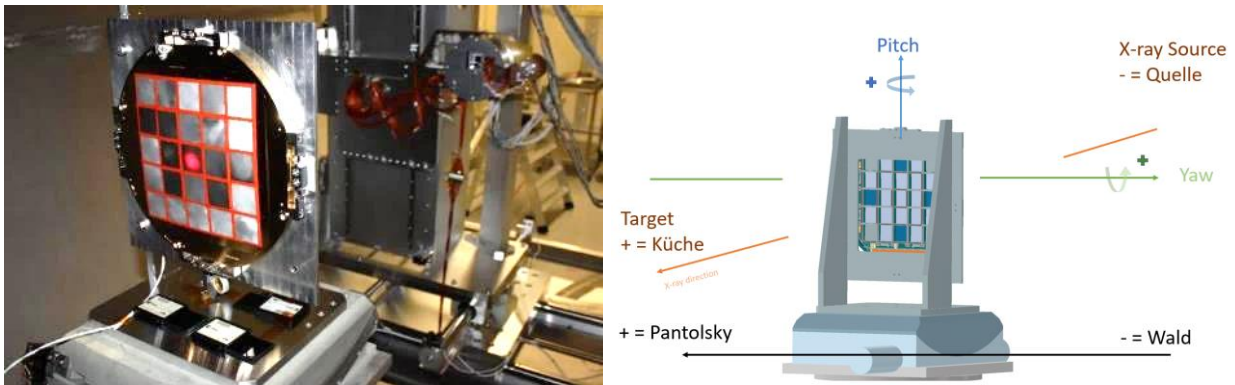


Figure 5 (left) The SVOM-MXT-MOP flight Model (FM) optics in the PANTER vacuum chamber, view from the source toward the detector is shown (right) the coordinate.

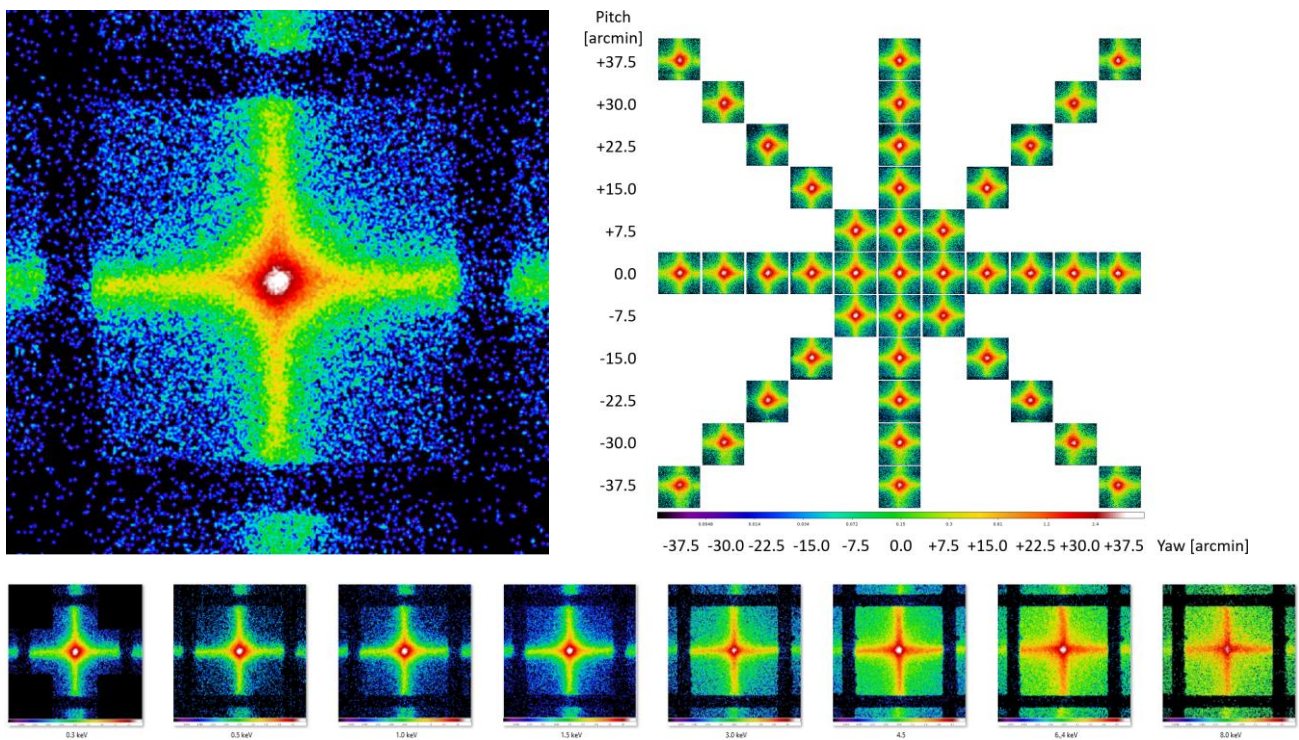


Figure 6 Measurements of the MXT-MOP-FM at Al-K (1.5 keV): (top left) a grid of 3 × 3 TRoPIC images combined to study the cross arms of the PSF in detail, (top right) a so-called focal plane map obtained to study variation of the PSF and efficiency of the optic on-axis as well as for a grid of off-axis angles. (bottom) the PSF as a function of energy is shown from left to right C-K, O-K, Cu-L, Al-K, Ag-L, Ti-K, Fe-K, Cu-K.

4.2 SVOM-MXT: Telescope Testing at PANTER

The goal of the SVOM-MXT tests at PANTER was to characterize the performance of the telescope by studying the on-axis and off-axis PSFs, measuring the energy-dependent efficiency (effective area) of the flight telescope under different thermal loads, with a different detector and optic temperatures, as well as testing the X-ray source localization algorithms. Furthermore, measurements with optical lasers, and laser trackers were combined with the X-ray measurements, allowing for an accurate determination of the line of sight (LOS) and characterization of optical loading on the detector (see Table 4). In addition, a verification of the thermal properties of the telescope was possible as for these tests a liquid nitrogen cooled shroud mounted above the telescope radiator was available (see Figure 7).

At PANTER, performance tests of two different models of fully integrated SVOM-MXT telescopes were done that included the optic, the detector, the radiator, and the camera plus telescope control electronics. The first so-called “Performance-Model (PM)” test was a combination of the QM optic and an engineering model (EM) detector, in this model the telescope tube was made of aluminum. This PM performance test took place during the first quarter of 2020 and was completed just prior to the onset of the covid-19 pandemic. The performance test of the Flight Model (FM) (see Figure 7) took place during the last quarter of 2021 when it became possible to travel again (but still under strict covid-19 regulations). For this test, all flight Model (FM) components (optic, detector, carbon fiber telescope tube, radiator and control electronics) were used.

Table 4 Overview of the SVOM-MXT telescope tests performed at the PANTER X-ray test facility. High-lighted in blue are the AHEAD 2020 activities

| Telescope Performance Tests | Date | Optic | Detector | Measurements |
|-----------------------------|-------------------------------|-----------|-----------|----------------------------|
| Laser alignment Test | July 2019 | --- | --- | Feasibility test |
| Performance Model (PM) | Jan. 20 – Feb 28, 2020 | QM | EM | Calibration (test run) |
| Flight Model (FM) | Oct. 05 -Nov. 19, 2021 | FM | FM | Calibration (final) |

The telescope in both tests was mounted on a tip-tilt (pitch) and rotary (yaw) stage which is visible under the telescope in (see Figure 8 bottom). This pair of stages was mounted on a translation stage that allowed for a side movement to be able to access the alignment laser with the optical cubes. The coordinate system used for the telescope test is described in Figure 8 right. The layout with distances in mm is shown in Figure 8 top. Due to the finite distance of the X-ray source, the image in the setup forms at 1 mm intra-focal (wrt to the nominal focus for a parallel beam). To be able to determine the effective area of the telescope, a Silicon Drift Detector (SDD) was installed 35 m from X-ray source to monitor and measure the X-ray flux its location is marked in Figure 8.

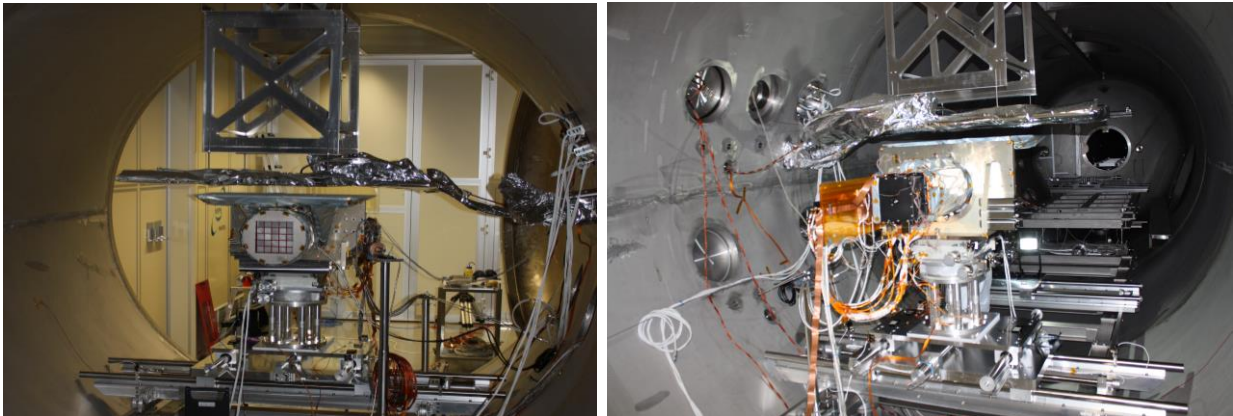


Figure 7 The PANTER thermal shroud and its MLI covering are visible above the MXT-FM. The MXT-FM model in the chamber, (left) with the MOP cover removed, prior to closing the chamber door and pumping down. Photo is taken looking from the direction of the X-ray source. (right) The detector end of the MXT inside the chamber, shortly before closing the chamber and pumping down. The PANTER thermal shroud and its MLI covering are visible above the MXT-FM. Photo is taken facing the X-ray source.

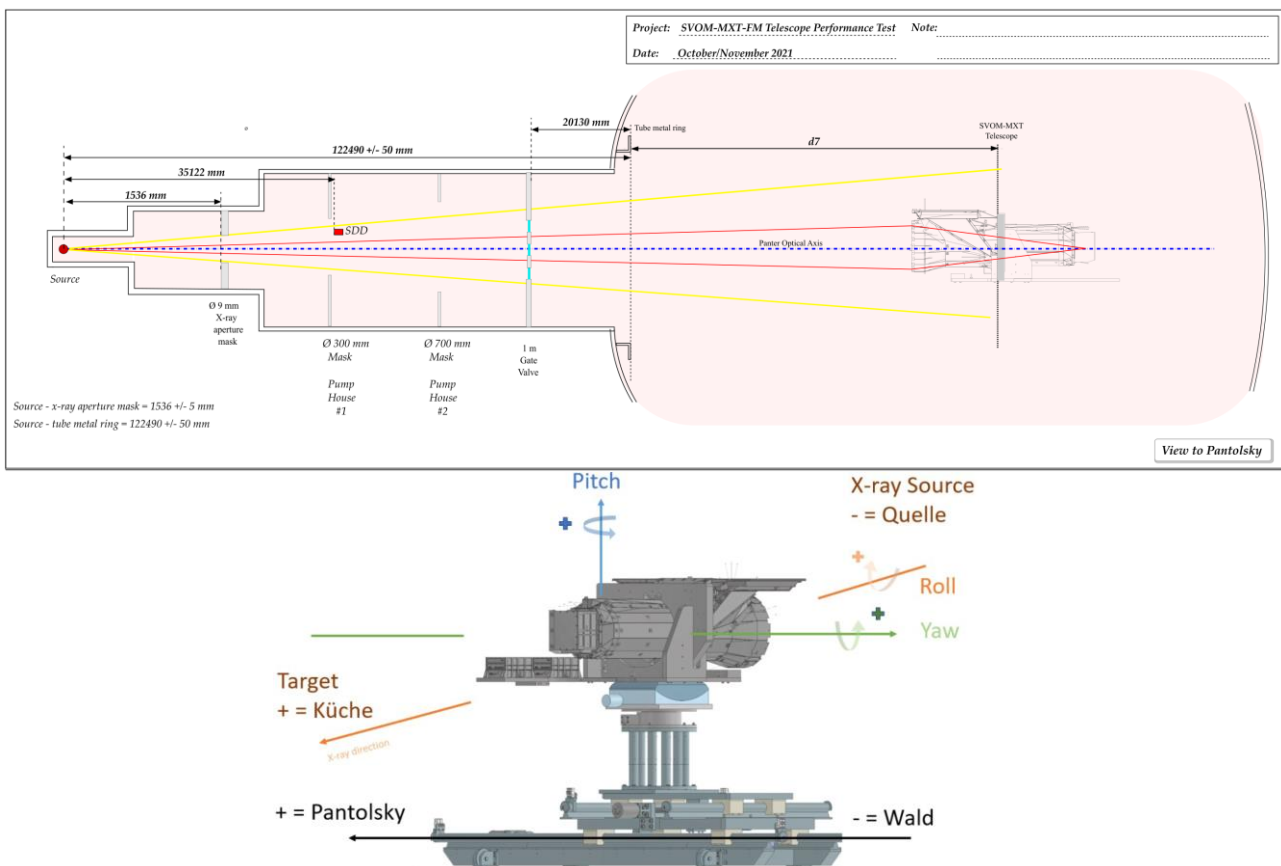


Figure 8 (top) Diagram showing the position of the Telescope, and the measurement position $d7 = 10282 \pm 2$ mm in the chamber. (bottom) shows the coordinate system used during the telescope tests.

In Figure 9 the positions used for measuring and characterizing the PSF are documented. The resulting effective area measured during SVOM-MXT-FM performance test is shown in Figure 10. Further results and final numbers will be presented in a paper by Diego Götz that is currently in preparation.

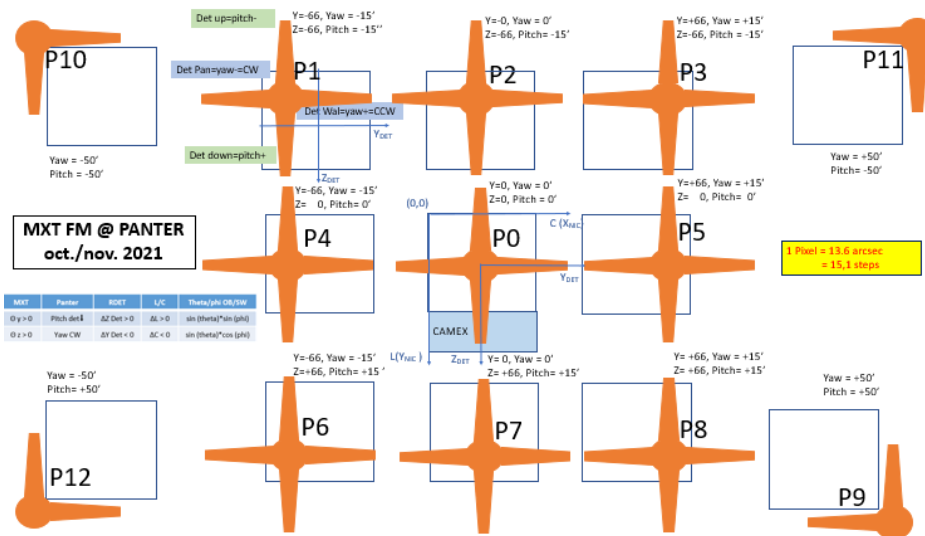


Figure 9 Measurement strategy showing the positions chosen for the location of the PSF on the detector with the corresponding pitch and yaw angles to which the telescope has to be oriented to.

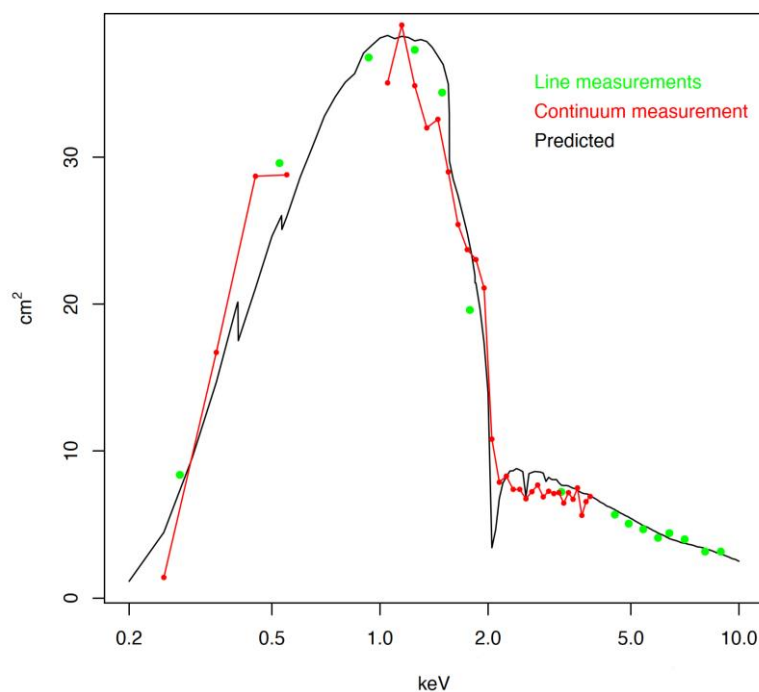


Figure 10 This plot shows the effective area of the SVOM-MXT-FM telescope as measured in PANTER during the performance tests: in green the effective area measurements at the characteristic lines of the X-ray source target elements available at PANTER, in red the continuum flux measurements and in black the effective area model prediction.

During the last seven years multiple measurement campaigns took place at the PANTER X-ray test facility of the Max Planck Institute for Extraterrestrial Physics to follow the development and calibrate the flight and flight spare optics of the SVOM-MXT. Furthermore, two highly elaborate performance test campaigns were successfully completed at PANTER to study the on-axis and off-axis PSFs, to measure the energy-dependent efficiency (effective area) of the flight telescope under different thermal loads, test the X-ray source localization algorithms for sources on the sky, as part of proving the flight control electronics, as well as to determine the line of sight of the telescope and quantify the optical loading. Since the end of 2021 all is set to deliver the SVOM-MXT-FM telescope to China for integration into the spacecraft for a launch in 2023.

4.3 Einstein Probe: FXT Optic Testing at PANTER

4.3.1 MEASUREMENT METHODS

X-ray Alignment: Burkert test

The Burkert test was carried out in full illumination in the double reflection position for a coarse alignment. The aim of the test was to align the optic in pitch and yaw using single reflections from the full MA. The optic was aligned iteratively, with alterations in pitch and yaw angle after the initial positions were observed. Although the Burkert test was performed under full illumination, only the single reflections from the innermost shell – Shell 54 – were used for alignment. A high beam intensity allows quick visualisation of the single reflection structures.

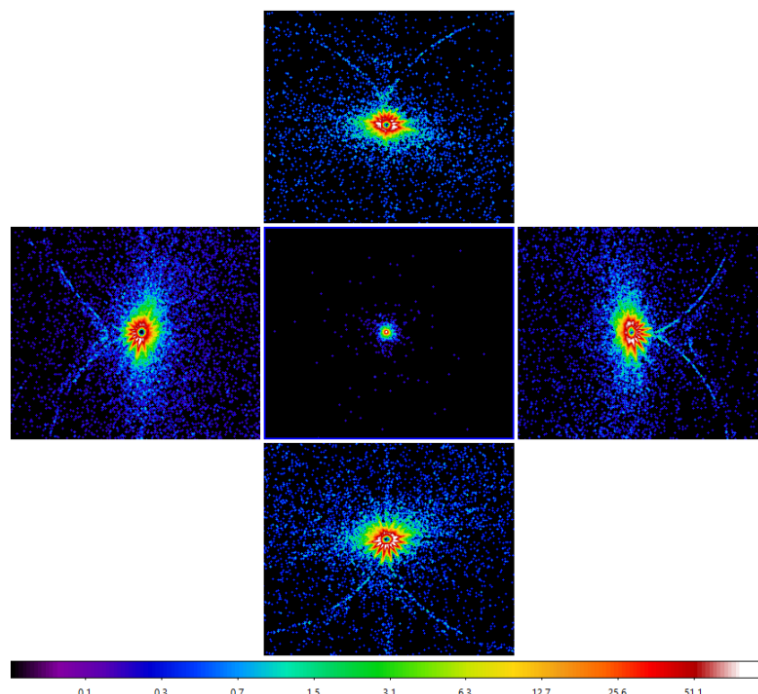


Figure 11 The Burkert test result at Al-K. Clockwise from top with angles relative to laser alignment: positive pitch (+19.0 arcmin), negative yaw (-20.1 arcmin), negative pitch (-16.0 arcmin), positive yaw (+15.5 arcmin). The central image is the resulting on-axis PSF, in preliminary best focus.

During the Burkert test, the higher-than-usual heating voltages led to a 'hole' at the centre of the double reflected image as shown in Figure 11. This is caused by the pile-up effect on the TRoPIC detector. For the Burkert test this 'hole' is acceptable, as only the geometry of the single reflection "arcs" with respect to the PSF centre is required.

X-ray Alignment: Egger-Menz Test

Once the Burkert test had preliminarily determined the best pitch and yaw angles, the Egger-Menz test was carried out to confirm these positions. This test determines the final best pitch and yaw angles, the on-axis position of the MA. Contrary to the Burkert test, the Egger-Menz test is sensitive to the full mirror system and not only for one shell. This test requires a pitch scan and a yaw scan of the optic, where at each pitch/yaw position an intra-focal image is taken. From each position the azimuthal intensity distribution of the image is determined. For a perfectly aligned mirror the intensity distribution is homogeneous, but for an off-axis angle the intensity distribution becomes elliptical. Using the phase and amplitude of the second Fourier component of each image, the amount of off-axis angle can be quantified. The detector was moved 60 mm intra-focal relative to the laser alignment position for these measurements. The Egger-Menz pitch scan was completed first and followed by the yaw scan. Using steps of 3 arcmin, the scans were made around the best Burkert pitch and yaw position from -15 arcmin to +15 arcmin, with 600 seconds integration time per position.

Focus search

In preparation of the detailed 6x6 pixel scans at different local distances, a rough focus search around the laser alignment nominal image distance position, with PIXI was conducted, in order to get a good starting point for the precise focus search with TRoPIC.

With the TRoPIC detector, the focus search is the scan along the optical axis at a series of intra- and extra- focal positions around the nominal in-focus position (the laser alignment position) to determine the minimum HEW of the MA, at the energy Al-K (1.49 keV). At each position a 6x6 pixel scan (step width 12.5 μm , corresponding to 10 manipulator steps) with an exposure of 60 seconds was performed with TRoPIC.

Effective Area

The effective area measurement is done using the "Glücksrad" for the on-axis quasi-parallel illumination. The "Glücksrad" is a mechanical device to be used in the PANTER X-ray test facility for the effective area measurements of eROSITA-like mirror modules – such as EP-FXT – with an almost parallel beam. It consists of two independently rotatable masks on the same rotation axis which allow the illumination of selectable sectors of the mirror module aperture as shown in Figure 12. It has a high precision angular positioning system and well defined zero-positions for each mask. The masks are mounted into a frame which is placed in front of the mirror module (on the same stage). The "Glücksrad" can be operated remotely in the PANTER vacuum chamber.

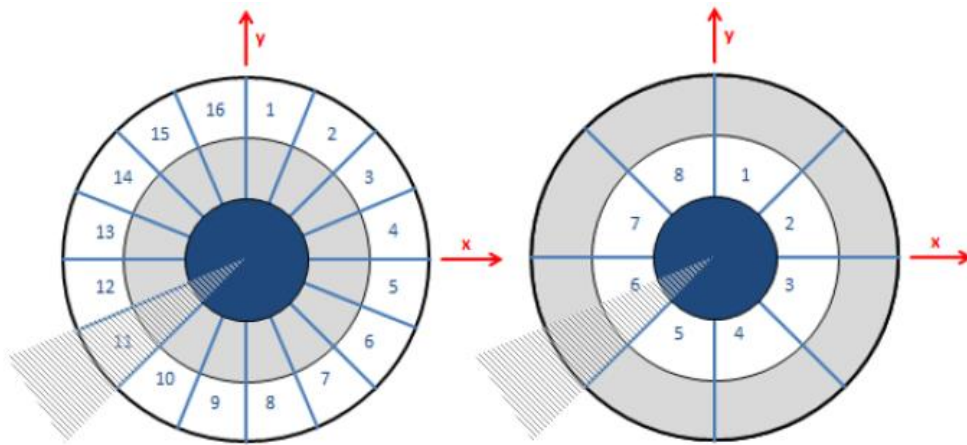


Figure 12 Sectors illuminated in almost parallel beam by the “Glücksrad” one after the other; left: outer sectors for shells 1 to 18 with 22.5 ° azimuthal width, right: inner sectors for shells 19 to 54 with 45 ° azimuthal width; the support structure of the “Glücksrad” blocks the outer sector 11 fully and half of the inner sector 6 (shaded area).

The measurements were carried out at five energies in on-axis and intra-focal position: Al-K (1.49 keV), Ag-L (2.98, 3.15, 3.35, 3.52 keV), Ti-K (4.51, 4.93 keV), Fe-K (6.4, 7.06 keV), Cu-K α (8.04 keV), and at the continuum energy ranges lEbc (0.8-4.0 keV), mEbc (2.35-8.0 keV). At each position an exposure was taken for approx. 5,000 counts. Before and after each measurement set a flat field (FF) exposure was taken, for approx. 1,500 counts. The flat field exposures serve as a reference for the X-ray beam, as the collecting area of detector is well defined; the region of interest of TRoPIC is 3.516 cm². During a flat field measurement, the optic and “Glücksrad” are removed from the X-ray beam, and TRoPIC remains in the on-axis, intra-focal position. The use of two flat field exposures accounts for possible beam variations over the measurement period. The effective area values in this report are corrected using the flat field exposures. Fifteen outer 22.5° sectors (shells 1 to 18) and eight inner 45° sectors (shells 19 to 54) were separately measured with TRoPIC. For each sector, the MA was turned in pitch/yaw such that the centre of the sector is perpendicular to the line-of-sight to the X-ray source.

This way the sector is illuminated with an almost parallel beam.

The effective area A_{eff} was calculated using Equation 1 , where C_{optic} is the count rate from the optic, C_{FF} is the flat field count rate, A_{det} is the collecting area of the detector (3.516 cm²), and G is the geometrical correction for the divergent X-ray beam.

$$\text{Equation 1} \quad A_{eff} = \frac{C_{optic}}{C_{FF}} \times A_{det} \times G$$

The geometrical correction, G , is calculated using Equation 2 , where the distance between the source and the optic is $d_{source-optic}$. The effective area is measured at the image distance d_{image} . The value for G for this campaign is 0.9734.

$$\text{Equation 2} \quad G = \left(\frac{d_{source-optic}}{(d_{source-optic} + d_{image})} \right)^2$$

The 1σ relative statistical error is calculated for each exposure, using the number of counts in the region of interest on the detector. This error is propagated through the above calculation to give a 1σ error on the effective area value of each exposure.

Deep PSF Exposures

The deep PSF images were made using the same pixel scan method described in Section 6.4.2. The detector was moved in Wald-Pantolsky and Up-Down in a 12×12 grid with a pitch of $6.25 \mu\text{m}$ scanning the in-focus on-axis PSF. over a full TRoPIC pixel – $75 \times 75 \mu\text{m}^2$. To avoid edge effects caused by TRoPIC's electronical signal processing components (one CAMEX for 128 pixel columns each) the image centre was positioned close to the "Zauberpixel" (pixel coordinates 104, 128), a sweet spot for the measurement due to the detector chips arrangement. The measurement is done at 3 photon energies: C-K (0.28 keV), Al-K (1.49 keV) and Cu-K α (8.04 keV). Each exposure (at each of the 12×12 positions) was 150 seconds in length. The count rate was adjusted to approx. 0.54 counts/s over the full relevant spectral band, i.e. line + bremsstrahlung in an area of 3×3 pixels on the detector in order to avoid pile-up signals that would falsify the PSF result. This type of measurement allows a deep detailed PSF measurement to be made, as scanning over the pixel avoids pattern type bias. This is necessary because the PSF is so small that the photons encircled in the "HEW circle" during the analysis are mainly detected in one pixel.

Focal Plane Mapping

The focal plane mapping (FPM) was done primarily to obtain a vignetting curve, but it also delivers some information on the off-axis PSF. The method uses several off-axis positions over a 1 degree by 1 degree field-of-view (FOV), which corresponds to the detector size used for FXT. The time consumption was kept relatively low, as each position gets only 80 seconds exposure time, while the source flux was maximized. The consequent high count rates cause pile-up, which however can be taken into account by the analysis software that adds up also all counts in the multiples of the used characteristic line. The FOV is covered by using two grids of data points, shown in Figure 13:

- 1) The wider grid consists of 8 by 8 positions that range from $-28'$ to $+28'$ in steps of $+8'$, both in yaw and pitch.
- 2) The smaller grid consists of 5 by 5 positions that range from $-6'$ to $+6'$ in steps of $+3'$, both in yaw and pitch.

Both grids are complementary since the wider one covers the entire course of the vignetting curve, while the smaller one reveals its central part. Both grids are centered on the measured optical axis, but the analysis of the FPM allows to correct this position. The detector position during FPM is fixed, since the mirror tilting in yaw and pitch lets the images always appear at (almost) the same location.

Before and after each of the scans (at least one) flat field measurements were done to monitor the X-ray beam. All FPM measurements were done at -0.4 mm intra-focal. The Glücksrad was put out of the beam in park position. The FPM was done at 5 energies: Al-K, Ag-L, Ti-K, Fe-K and Cu-K. Note that for Fe-K and Cu-K a different gain setting of the TRoPIC detector was used (gain EC) in order to extend the measurable energy band such that all relevant pile-up peaks could be found.

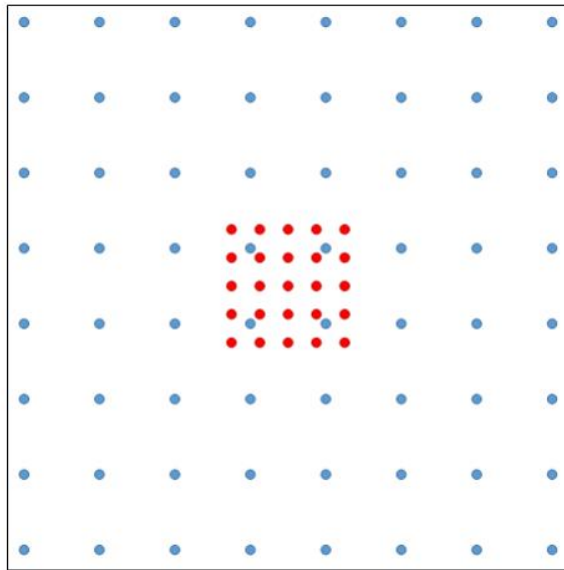


Figure 13 The two grids for focal plan mapping in a 60 arcmin \times 60 arcmin square.

Focal Length Measurement

After the final set of X-ray measurements, the detector was moved into the best focus position, on axis. The chamber was vented, and the focal length measurement was performed. The mechanical-optical gauge⁸ was inserted in the MM's blocking shell and positioned to measure the distance between the MM's reference mirror (in the centre of the spider wheel) and the detector CCD chip. The detector was moved incrementally towards the gauge until it was detected by the gauge sensor, ensuring no damage to the CCD chip. The range of the sensor is up to 2500 μm . Reference measurements were done before and after, using a standard that had been calibrated with a coordinate measuring machine to an accuracy of 5 μm . Due to the uncertainty of the exact position of the principal plane of the optic, the focal length can be determined with an accuracy of 0.5 mm only. However, more important is the knowledge of the distance between the reference mirror and the the surface of the CCD chip, which can be determined with an accuracy of about 40 μm . This distance will be used during the assembly of the FXT, when optic and detector are mounted into the telescope structure.

4.3.2 RESULTS

The measurement results for the Einstein Probe FXT QM are presented in this section. Effective area, Focal plane mapping and deep exposures.

Focus Search

The measurement result of the focus search is obtained from moving the detector around the rough best focus position in the range of $\pm 6\text{mm}$ along the optical axis. PSF analysis combines the 6x6 pixel scan for each position. The resulting focus curve (HEW vs focus position 'A17') is then fitted with a hyperbola fit as shown in Figure 7 where the minimum HEW of 23.4 arcsec corresponds to the best focus position.

Deep PSF Exposures

This measurement allows a deep detailed PSF measurement to be made, as scanning over the pixel avoids pattern type bias. This is necessary because the PSF is so small that the photons encircled in the "HEW circle" during the analysis are mainly detected in one pixel. The results summary of the on-axis deep PSF measurement is in Table 2. Sets of images were taken with PIXI at intra- and extra- focal position to observe the defects and deformation in Figure 8. This is caused by the either vibration or thermal test, on the mirror shells. The intra-focal images were taken at -80 mm and the extra-focal images were taken at +80 mm from the best focus position.

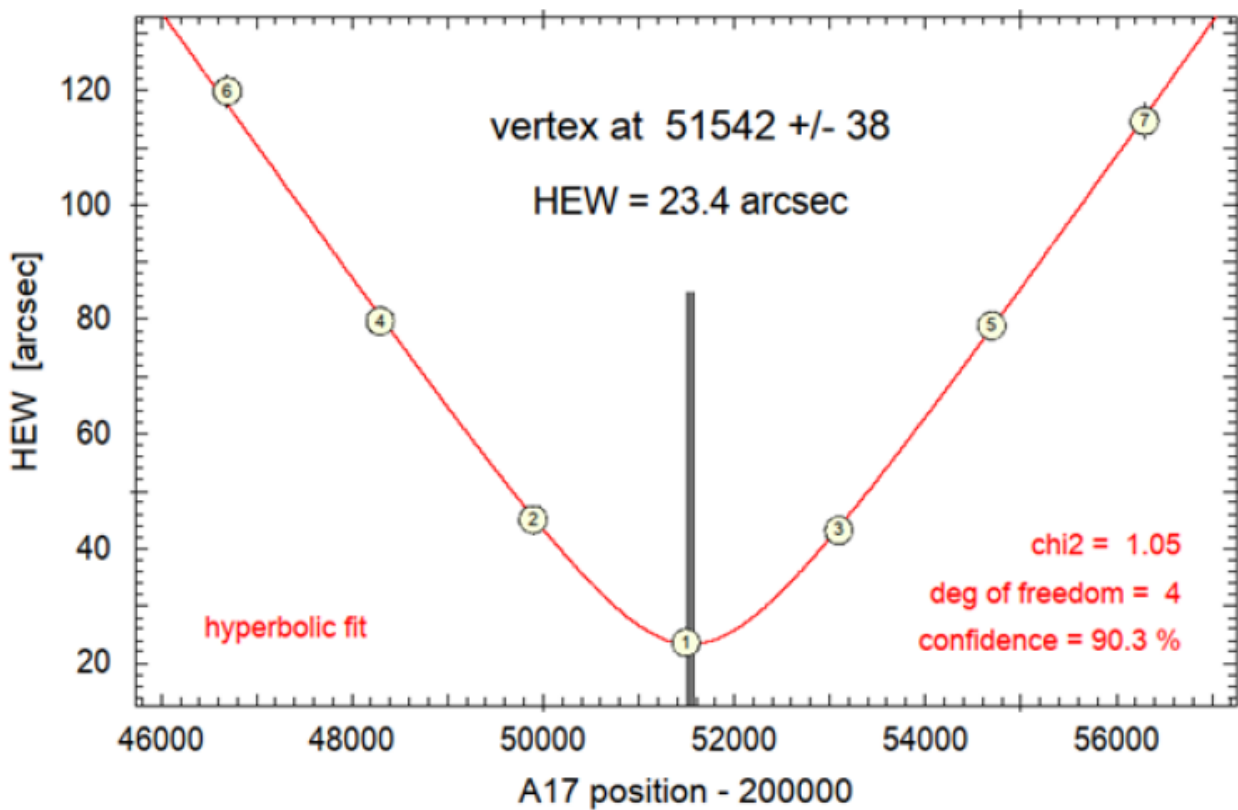


Figure 14 The compilation results of the focus search and the hyperbola fit to determine the best focus position, the smallest PSF (minimum of HEW), for the QM at Al-K.

Table 2. Summary of the Deep PSF measurement at different energies for the QM.

| Energy | HEW (arcsec) | W90 (arcsec) | Scattering Fraction |
|--------|--------------|--------------|---------------------|
| Al-K | 23.8 ± 0.3 | 117.3 | 0.057 |
| Cu-K | 25.7 ± 0.4 | 323.8 | 0.203 |
| C-K | 23.8 ± 0.4 | 100.6 | 0.040 |

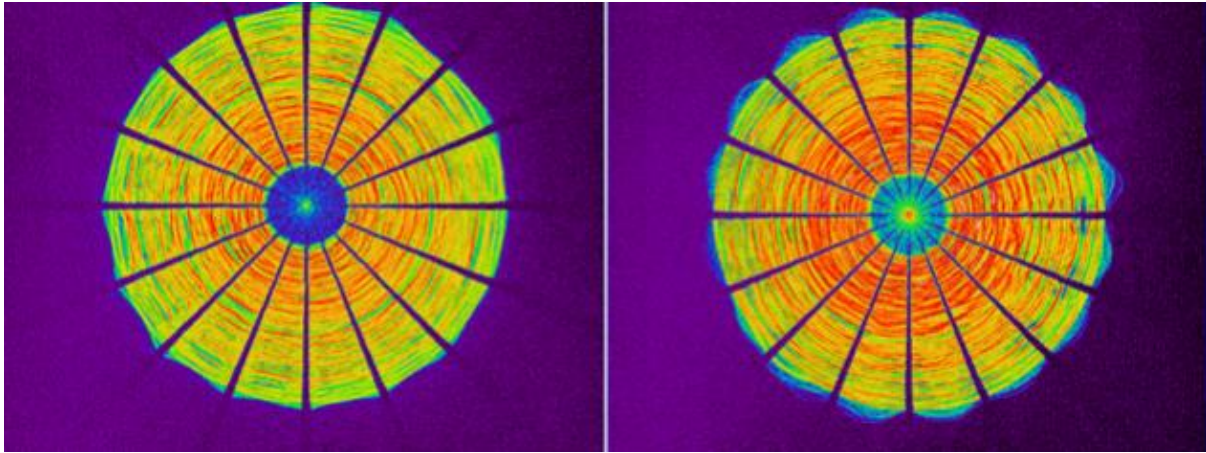


Figure 15 The compilation of images of the deep PSF of the QM at Al-K with PIXI intra- (left), and extra-focal (right).

Effective Area

The effective area measurements with the Glücksrad were carried out at -50 mm intra-focal position and illuminating all 8 inner- and 16 outer sectors one after the other in an almost parallel beam. The measurement at Al-K, Ag-L, Ti-K energies were carried out for both inner and outer sectors while at Fe-K and Cu-K were done only for the inner sectors. The compilation of images at each energy is displayed in Figure 9 with the summary of the effective area at inner sectors, outer sectors and the full optic is in Table 3. The summary on the low energy band continuum measurements is shown in Figure 10. The measured data points at different energies were plotted over the continuum measurement at IEbc.

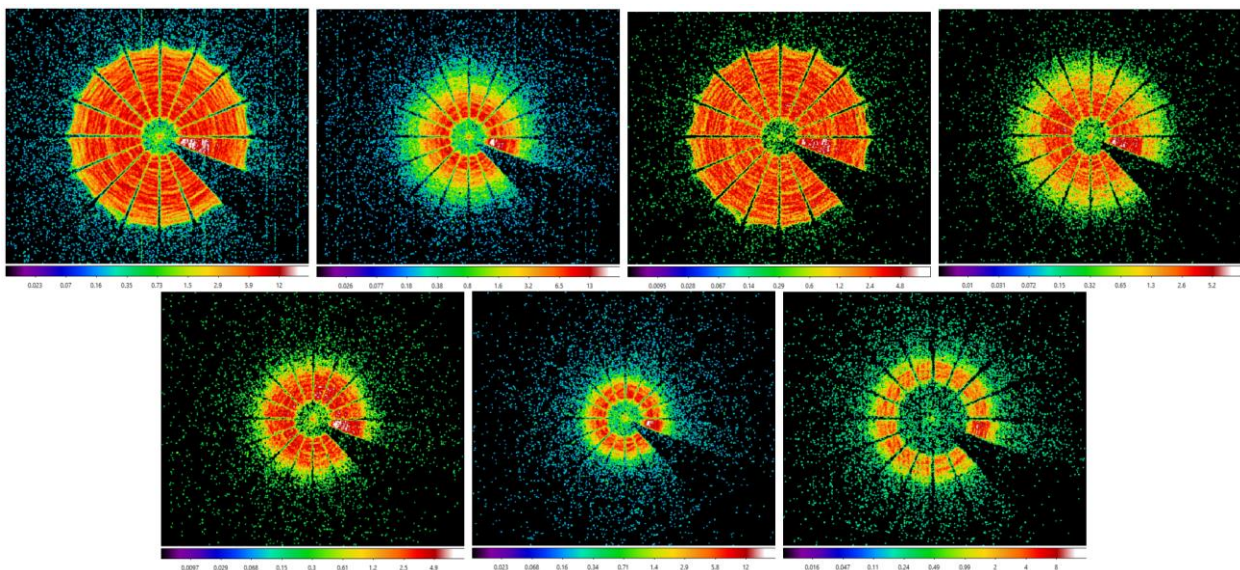


Figure 16 Compilation of intra-focal images for different sectors of the QM MA selected by different positions of the "Glücksrad" at different energies: (Top row) IEbc, mEbc, Al-K, Ag-L (Bottom row) Ti-K, Fe-K, Cu-K respectively, for the qualification model. Sector 11 is fully obscured by the support arm of the "Glücksrad".

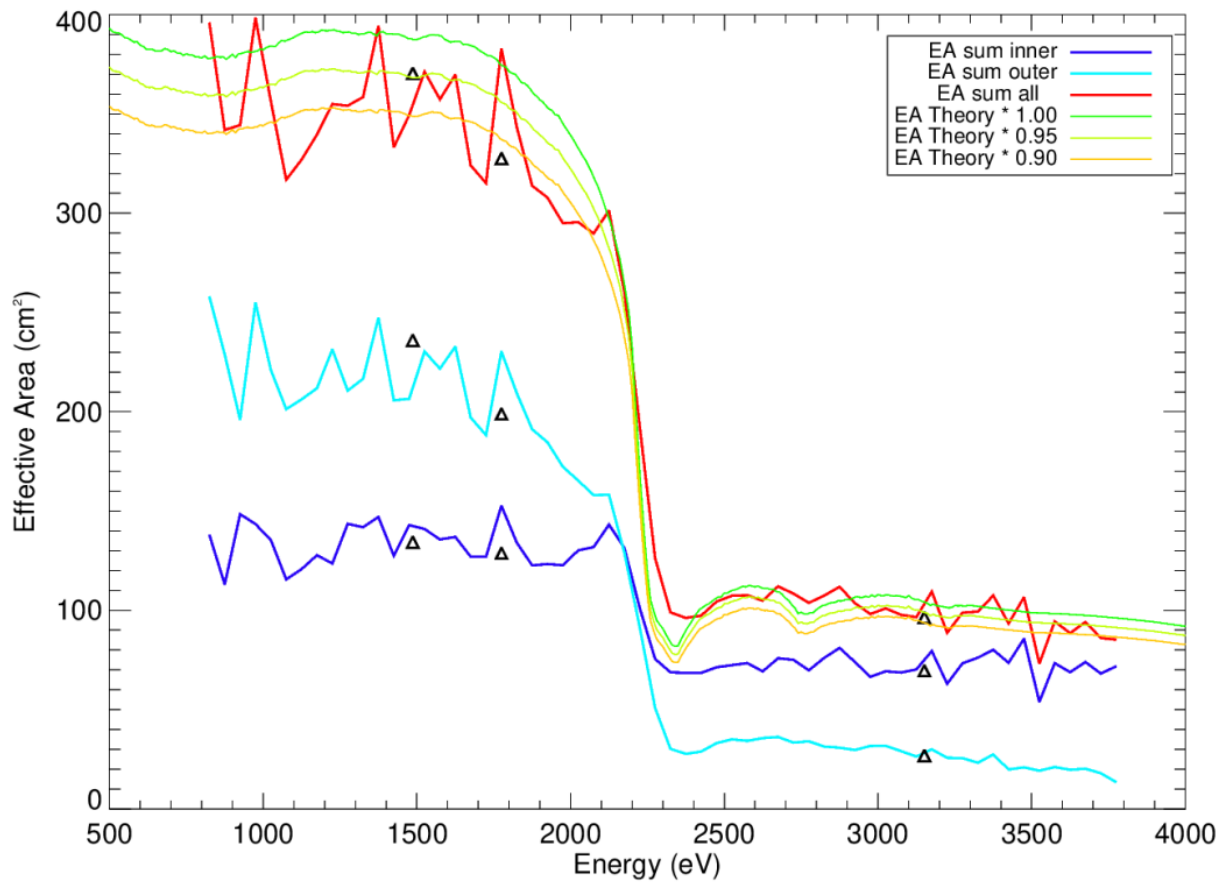


Figure 17 The effective area measurements of the QM MA overlaid with the theoretical model. The summary of effective area at low energy band continuum at different sectors are shown with different color: dark blue for inner sectors, light blue for the outer sectors and red for the total mirror. The small triangles are the measured data points for the energies Al-K, W-M and Ag-L.

Table 3. Summary of the effective area at different energies, for the QM

| Energy | Inner Sectors | Outer Sectors | Total (full optic) |
|--------|-------------------|-------------------|--------------------|
| Al-K | 134.42 ± 2.28 | 236.08 ± 2.93 | 370.50 ± 3.72 |
| Ag-L | 69.58 ± 0.54 | 26.81 ± 0.24 | 96.39 ± 0.60 |
| Ti-K | 62.54 ± 0.82 | 3.86 ± 0.08 | 66.40 ± 0.82 |
| Fe-K | 33.52 ± 0.21 | - | 33.52 ± 0.21 |
| Cu-K | 18.18 ± 0.33 | - | 18.18 ± 0.33 |

Focal Plane Mapping and Vignetting

The results from the two overlapping grids, as described in 3.4, are shown in Figure 18. The FPM measurements, all in 0.4 mm intra-focal position and with boosted count rate, were performed for 5 photon energies: Al-K (1.49 keV), Ag-L (2.98 keV), Ti-K (4.51 keV), Fe-K (6.40 keV), Cu-K α (8.04 keV).

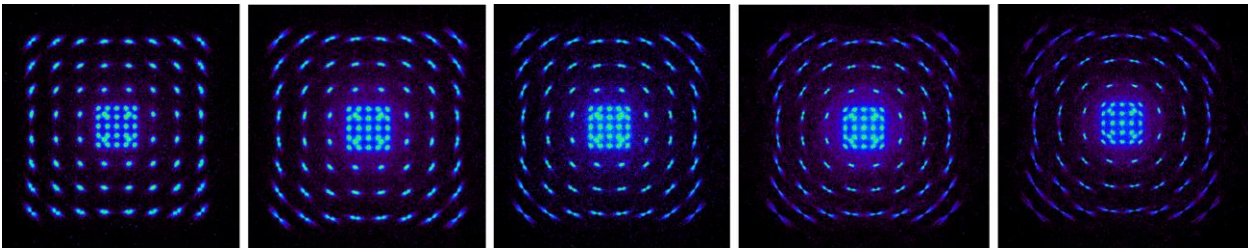


Figure 18 Composed focal plane mapping at different energies (left to right) Al-K, Ag-L, Ti-K, Fe-K, Cu-K respectively for the QM.

The vignetting curves for these 5 energies are derived from the FPM by analysing the count rates in each of the 89 off-axis positions, resulting in count rates as a function of off-axis angle. Finally, a fitting function is applied with the on-axis position as a free parameter. Figure 19 shows the normalised vignetting: As expected, the vignetting becomes steeper with increasing energy. Due to the large number of positions the curves are well defined, without being harmed by a few outliers.

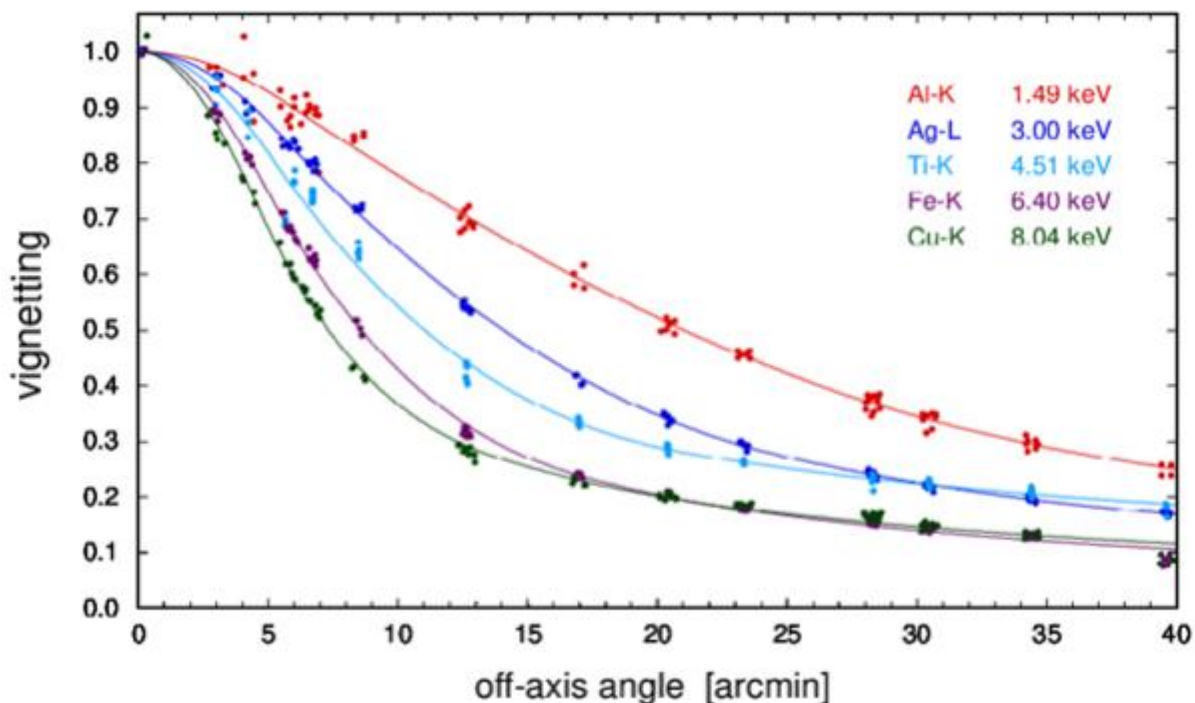


Figure 19 Vignetting curves for all five energies: Al-K, Ag-L, Ti-K, Fe-K, and Cu-K in comparison for the QM.

Focal Length Measurement

The measured distance between the MA reference mirror and the CCD chip (in focus) is 1792.870 mm \pm 0.021 mm. Applying several corrections, the target value of this distance in the orbit case is calculated as 1773.182 mm \pm 0.040 mm. The focal length is derived with less accuracy because of uncertainties about the exact position of the MA principal plane. The derived focal length of the QM MM is 1601.63 mm \pm 0.5 mm

4.3.3 DISCUSSION EP-FXT

Here we report the full calibration tests at different energies for the Einstein Probe FXT – QM at the PANTER X-ray test facility. The X-ray calibration test was done after the thermal cycling and vibration tests. They reflect the measured optical performance of the QM Mirror Assembly under laboratory conditions prior to delivery to China for further testing. Beyond the optical performance listed in the Table 5, the calibration includes many more measurements at different photon energies, which are reported in detail in the previous sections. The effective areas were measured using the “Glücksrad”, a device that allows measurements with a quasi-parallel beam that simulates almost the situation in orbit, where X-ray sources are at an “infinite” distance.

Table 5 Summary of the calibration measurements for the FXT QM and FM

| | Orbit | PANTER | QM |
|---------------------------------|-----------------------|-------------------------|-----------------------------------|
| HEW Al-K (1.49 keV) | <22" | <22" | 23.8 \pm 0.3" |
| HEW Cu-K (8.04 keV) | - | - | 25.7 \pm 0.4" |
| Eff. Area Al-K | > 350 cm ² | > 348.2 cm ² | 370.50 \pm 3.72 cm ² |
| Eff. Area Cu-K | > 20 cm ² | > 18.7 cm ² | 18.18 \pm 0.33 cm ² |
| Micro-roughness Scattering Cu-K | < 0.5 nm | < 15.7 % | 20.3 % |
| Focal length | 1600 \pm 2 mm | 1600 \pm 2 mm | 1601.63 \pm 0.50 mm |

For the QM, the optical performance in terms of HEW degraded slightly during the thermal cycling test, while there was no performance change after vibration as seen at the STM MA [11]. A reduction of the on-axis effective area at high energies was observed after the mounting of the X-ray baffle; this is due to the tight nesting of the inner mirror and baffle shells, where a slight misalignment can cause partial shading. There are a number of possible error contributions that finally reduce the optical performance. The required measurement results are summarized in Table 5. In conclusion, the QM telescope experienced a slight degradation of the half energy width (HEW) at Al-K energy (1.49 keV) during the thermal cycle which led to a slightly higher HEW than required but the QM satisfied the effective area requirement at the standard energy as well as the focal length.

4.4 Einstein Probe: WXT Optic Testing at PANTER

4.4.1 SETUP & ALIGNMENT

The coordinate system for the optics when mounted in the chamber is diagrammatically portrayed in Figure 20. An aperture of 5.5 mm was mounted 1.5 mm from the X-ray source. For a source-detector distance of 130 m, this aperture creates a beam with a diameter of approx. 440 mm at the optic. A movable mask is mounted in front of the optic. The mask has 130 × 130 mm size to cover the mount frame so that the reflections from the mount frame/housing do not contaminate the measurement. With the nominal focal length of 375 mm, the derived distance, for the PANTER facility, from the Küche side of the optic to the detector chip becomes 309.5 mm.

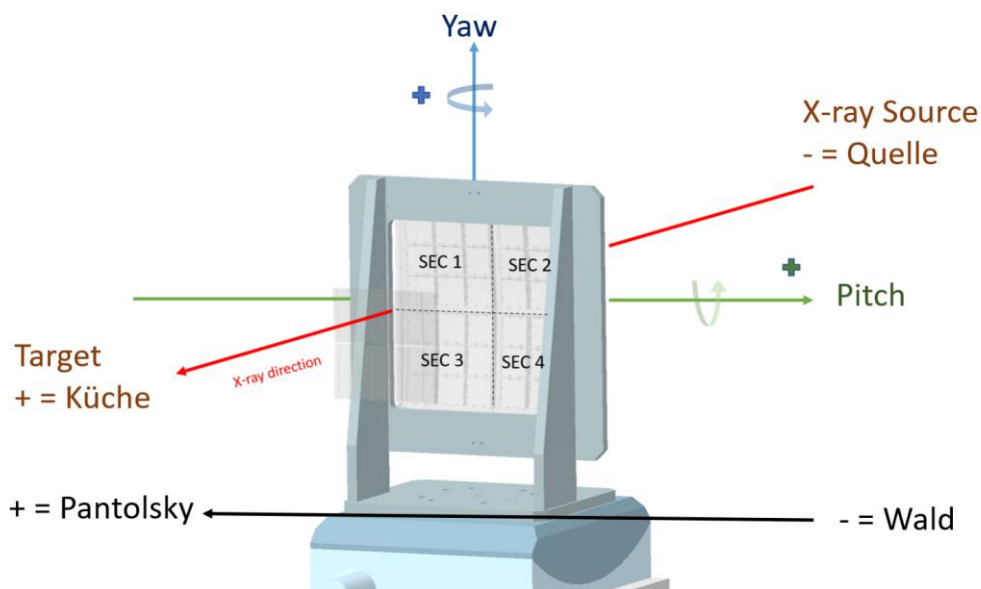


Figure 20 The PANTER coordinate system. The EP-WXT is mounted on the manipulator. The different sectors are labeled.

Alignment

To make the alignment of the X-ray image on the detector easier, alignment using a visible laser is carried out before the chamber is closed and put under vacuum. The laser is mounted in the same position as the X-ray source and the beam travels down the same beam-line to the optics. A metal cross-bar, made for the QM MOP campaign, was re-used as the central section of the MOP interface plate, to assist with the alignment of the frame in the chamber. The interface plate was mounted in the chamber and translated in Wald-Pantolsky until the alignment laser was visible on the cross-bar. Once the interface plate was aligned to the laser, the MOP was mounted to the interface plate. The laser position is visible on the MOP in Figure 21 at the center of the MOP. This was noted as the 'laser alignment' position of the MOP. Later this position was recorded under X-ray beam as a reference position. The corresponding image is shown in Figure 22 on the right side of the image where the left side is the simulated result of the intersection of the four sectors in the middle of the mirror module.

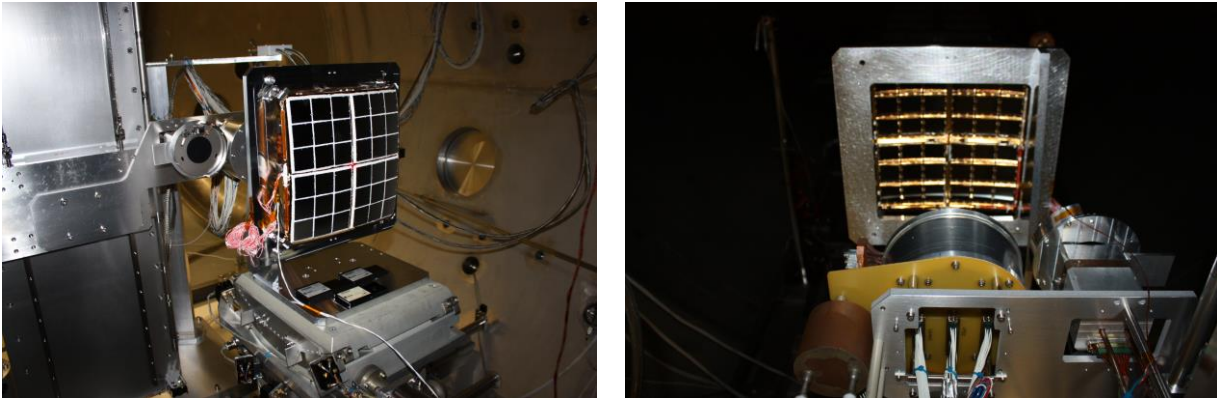


Figure 21 The WXT installed inside the PANTER chamber. (Left) The MPO mounted in the chamber, with the alignment laser centred on the MPO and the TRoPIC camera visible in the background (photo taken facing Pantolsky-Küche. (Right) The back side of the MPO inside the chamber.

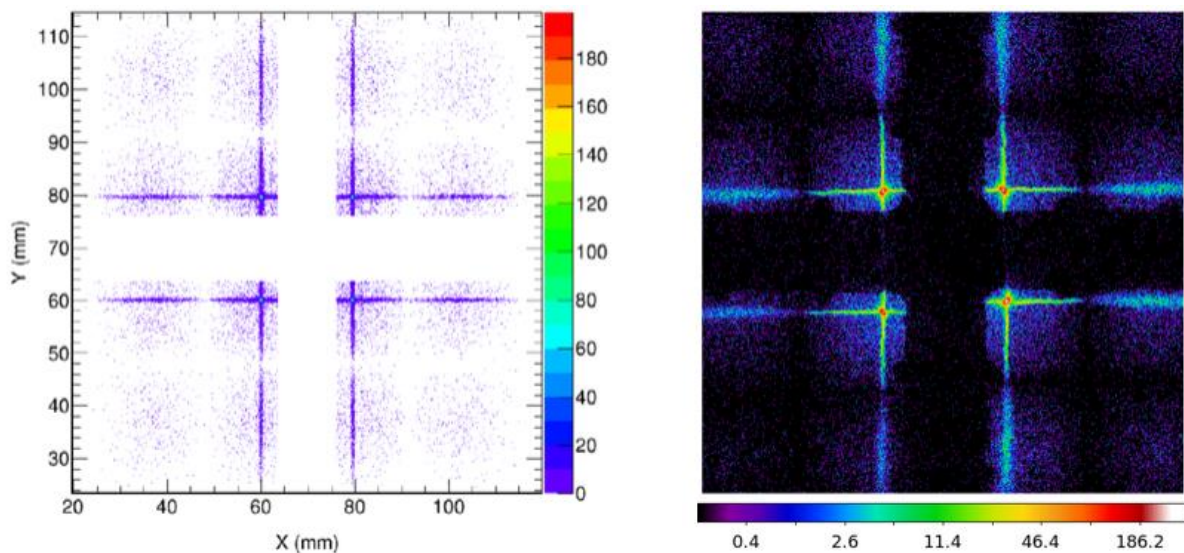


Figure 22 The first image of alignment under X-ray (right) compare to the simulated result (left)

4.4.2 MEASUREMENT METHODS

Focus search

A focus search was made at Cu-L, Ti-K, C-K, very low Energy band continuum (vIEbc), and low Energy band continuum (lEbc). The optic was moved in Quelle-Küche by ± 12 mm in 4 mm steps around the nominal focus position. The count rate was recorded for each position. For this campaign, the FWHM was used as the focus search metric, and was calculated by fitting a simple Gaussian function to the profile curves in x- and y-direction of the PSF image. The minimum of the best fit (FWHM $(x+y)/2$ and relative position) was taken as the best focus position. The analysis has been done independently by the PANTER team and the by University of Leicester (UoL) team. The UoL focus position was used as the 'best focus' position for the campaign.

On-Axis Extended Mosaic PSF

An extended PSF image was made at energies: Cu-L, Ti-K and vIEbc to characterise the extended arms of the on-axis PSF. This is a 3 × 3 TRoPIC scan of the on-axis in focus PSF. The nine images are then combined into one ‘mosaic’ image, to show the full PSF. The image size is 3 × 3 × 18.6 × 18.6 mm (approx. 3 TRoPIC FOVs, with a 600 µm overlap corresponds to 18.6 × 18.6 mm² (19.2 × 19.2 mm² is the whole TRoPIC size).

Focal plane mapping

Focal plane mapping was carried out at each energy. The optic was moved into the best focus position and tilted in yaw by ±150 arcmin in 50 arcmin steps, whilst remaining in best pitch position. The detector was translated in Wald-Pantolsky to follow the PSF. The pitch was then altered by ±150 arcmin in 50 arcmin steps, with the optic in best yaw position. Once these two sets of measurements had been made, the first diagonal scan was made. The pitch and yaw were both altered by ±150 arcmin in 50 arcmin steps (e.g., -150 arcmin pitch and -150 arcmin yaw). The second diagonal scan of alternating pitch and yaw positions (i.e., +150 arcmin pitch and -150 arcmin yaw) was made. These four scans allowed a map of the focal plane to be made. Each position exposure was 300 seconds. These four scans allowed a ‘map’ of the focal plane to be created. For the key energies (Cu-L, C-K, and Ti-K) the full range was used.

Effective Area

The effective area A_{eff} was calculated using Equation 3, where C_{optic} is the count rate from the optic, CFF is the flat field count rate, A_{det} is the collecting area of the detector (3.516 cm²), and G is the geometrical correction for the divergent X-ray beam.

$$\text{Equation 3} \quad A_{eff} = \frac{C_{optic}}{CFF} \times A_{det} \times G$$

The geometrical correction, G , is calculated using Equation 4, where the distance between the source and the optic is $d_{source-optic}$. The effective area is measured at the image distance d_{image} . The value for G for this campaign is 0.994.

$$\text{Equation 4} \quad G = \left(\frac{d_{source-optic}}{(d_{source-optic} + d_{image})} \right)^2$$

The 1σ relative statistical error is calculated for each exposure, using the number of counts in the region of interest on the detector. This error is propagated through the above calculation to give a 1σ error on the effective area value of each exposure.

Flat field

A flat field exposure was taken before and after each measurement set. The flat field exposures serve as a reference for the X-ray beam, as the collecting area of detector is well defined; the region of interest of TRoPIC is 3.542 cm². During a flat field measurement, the optic is removed from the X-ray beam, and TRoPIC remains in the on-axis, in-focus position. The use of two flat field exposures accounts for possible beam variations over the measurement period. Multiple flat field exposures allow analysis of the beam stability over hours. The optic was moved out by 300 mm to Pantolsky in this campaign. Each flat field exposure was 900 seconds.

During the flat field and effective area measurements, the beam stability was also monitored. This provides an overview of how much the count rate of the X-ray beam at that energy fluctuated over a specific measurement period.

4.4.3 RESULTS

Focus search

A focus search of the full optic was carried out for the following energies: Cu-L and Ti-K. The analysis of the focus search were carried out independently from the PANTER team and the UoL team – see Table 6. It was decided to use the best focus of the UoL for this campaign. The off-axis focus search was done at sector 2 at various combinations: off-axis $\pm 2.5^\circ$ yaw, off-axis $\pm 2.5^\circ$ pitch, off-axis -2.5° pitch and -2.5° yaw, off-axis $+2.5^\circ$ and $+2.5^\circ$ yaw. The PSF images are fitted with a 2D Gaussian for the FWHM. The focus search of each sector, with the calculated FWHM, is plotted against the corresponding axis position in Figure 23. The focus axis DETQK = 26416 steps correspond to focal length of 375 mm at infinity. This includes a 9.5 mm shift due to the rotation of the optic by 5.4° in pitch and yaw to each sector with respect to 0° alignment of complete optic.

Table 6 Summary of the focus search result and analysis at Cu-L

| Sector | Focus PANTER | Focus UoL | Δf | Δf | FWHM(x/y) | f PANTER | F infinity |
|--------|--------------|-----------|------------|------------|-----------|----------|------------|
| (#) | (steps) | (steps) | (mm) | (mm) | (arcmin) | (mm) | (mm) |
| 1 | 26256 | 26624 | 368 | 0.46 | 4.4 | 373.8 | 375 |
| 2 | 24359 | 24358 | -1 | 0.00 | 4.7 | 371.4 | 372 |
| 3 | 22543 | 22351 | -192 | -0.24 | 3.8 | 369.2 | 372 |
| 4 | 22351 | 23099 | 1479 | 1.85 | 3.4 | 368.0 | 369 |

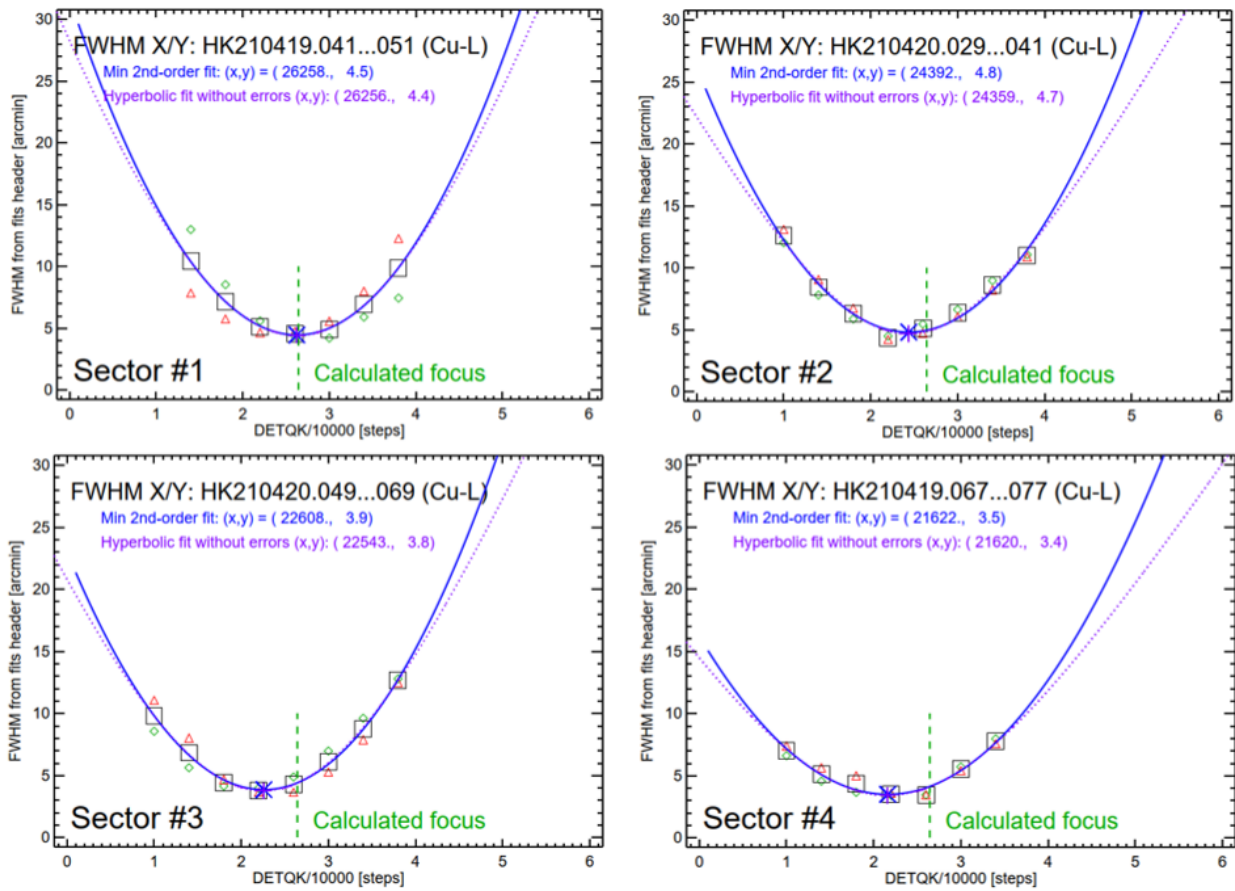


Figure 23 The focus search at Cu-L (PANTER analysis) for all sectors, with the calculated FWHM plotted against the corresponding axis position. The blue cross indicates the fitted best focus position. The green diamonds are the FWHM in x and the red triangles are the ones in y, from a simple Gaussian fit.

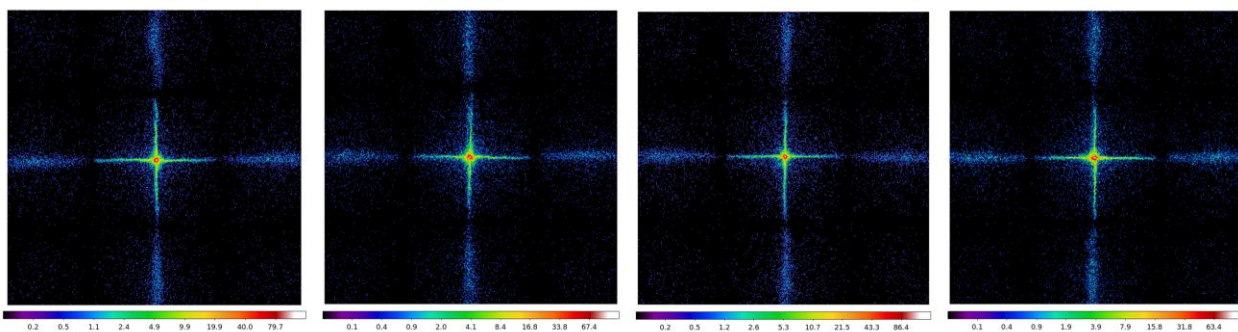


Figure 24 Compilation image of the on-axis in focus, extended (3x3) mosaic for each of the four sectors at Cu-L, from left to right are the PSF from sector 1 to 4 respectively.

On-Axis Extended Mosaic PSF

For each of the four sectors, a 3x3 scan was made to characterise the PSF at Cu-L (Figure 5) in best pitch and yaw position and in best focus position. The additional mosaic PSF images were carried out for sector 1 and 2 at Ti-K and vLEbc as shown in Figure 6 and 7.

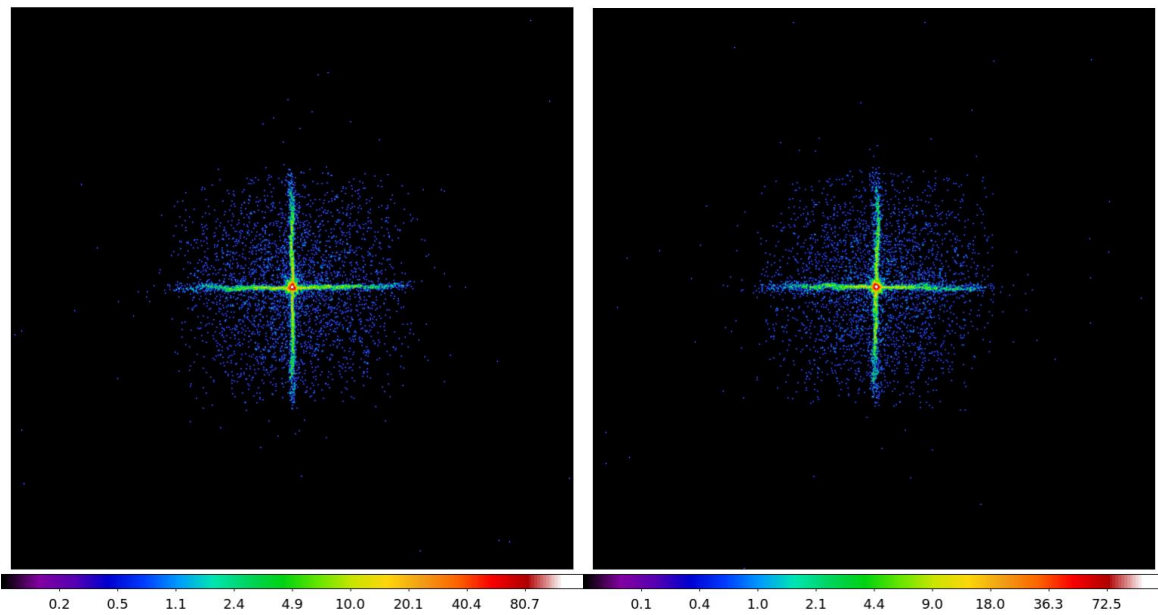


Figure 25 Compilation image of the on-axis in focus, extended (3x3) mosaic of the two sectors at Ti-K for section 1 (left) and sector 2 (right).

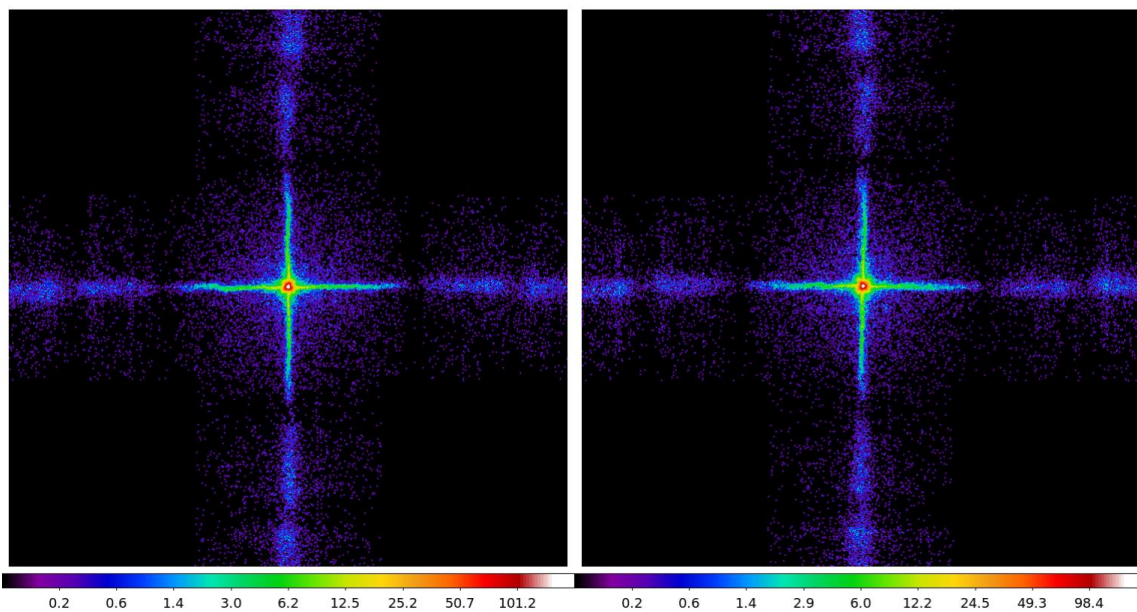


Figure 26 Compilation image of the on-axis in focus, extended (3x3) mosaic of the two sectors at vLEbc for section 1 (left) and sector 2 (right).

Focal Plane Mapping

Setting different pitch and yaw combination, the PSFs are mapped out on the focal plane both on axis and off-axis position. The scans were carried out in horizontal, vertical and diagonal directions from -150 arcmin to +150 arcmin as shown in Figure 27 at Cu-L. The missing positions from the bottom of sector 3 and 4 are due to the setup limitation. The focal plane mapping was also carried out at two additional energies: C-K and Ti-K in horizontal and vertical direction as shown in Figure 28.

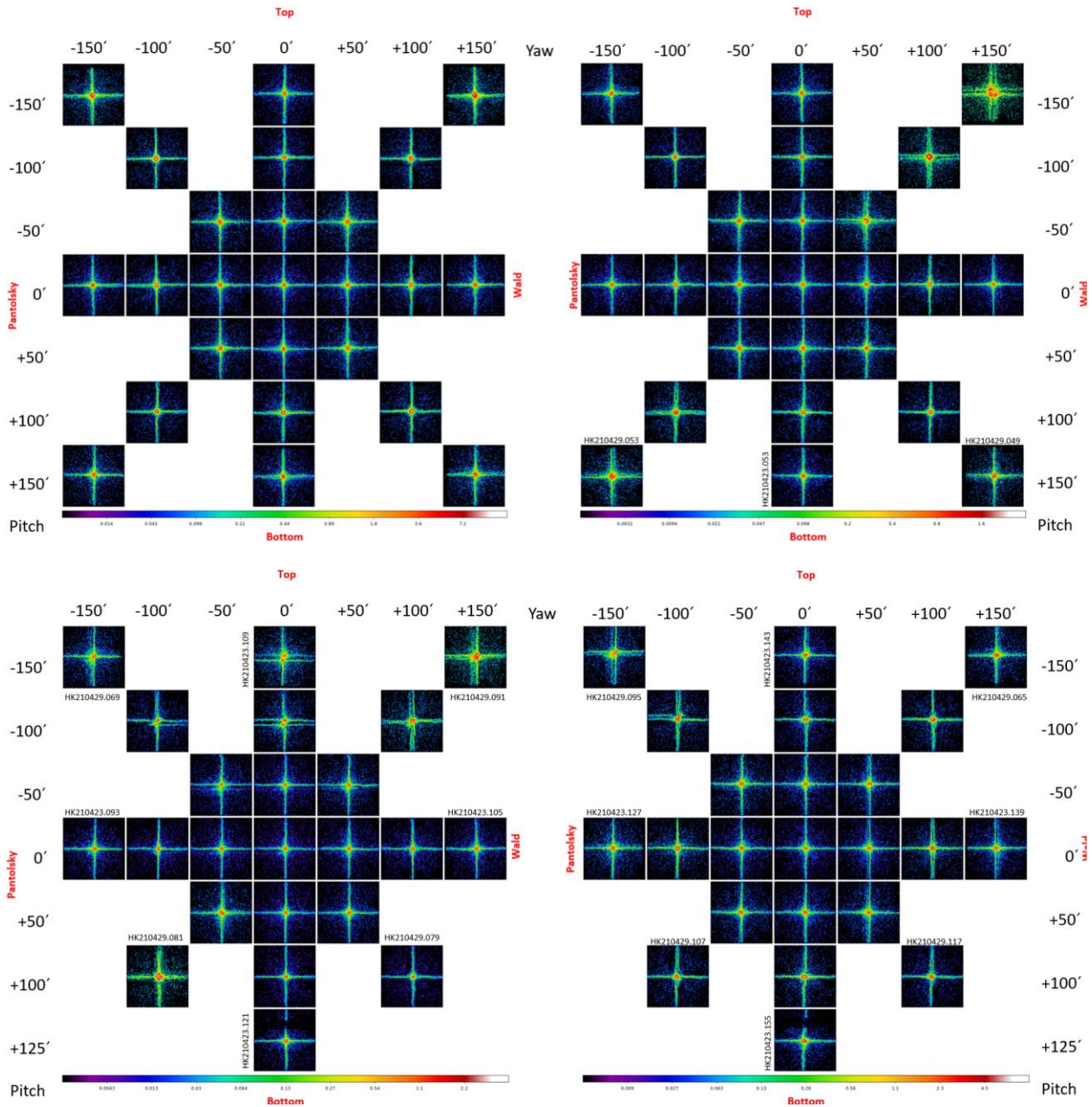


Figure 27 Compilation of PSF exposures for the focal plane mapping at all sectors: sector 1 (top left), sector 2 (top right), sector 3 (bottom left), sector 4 (bottom right) in horizontal, vertical and diagonal direction Cu-L.

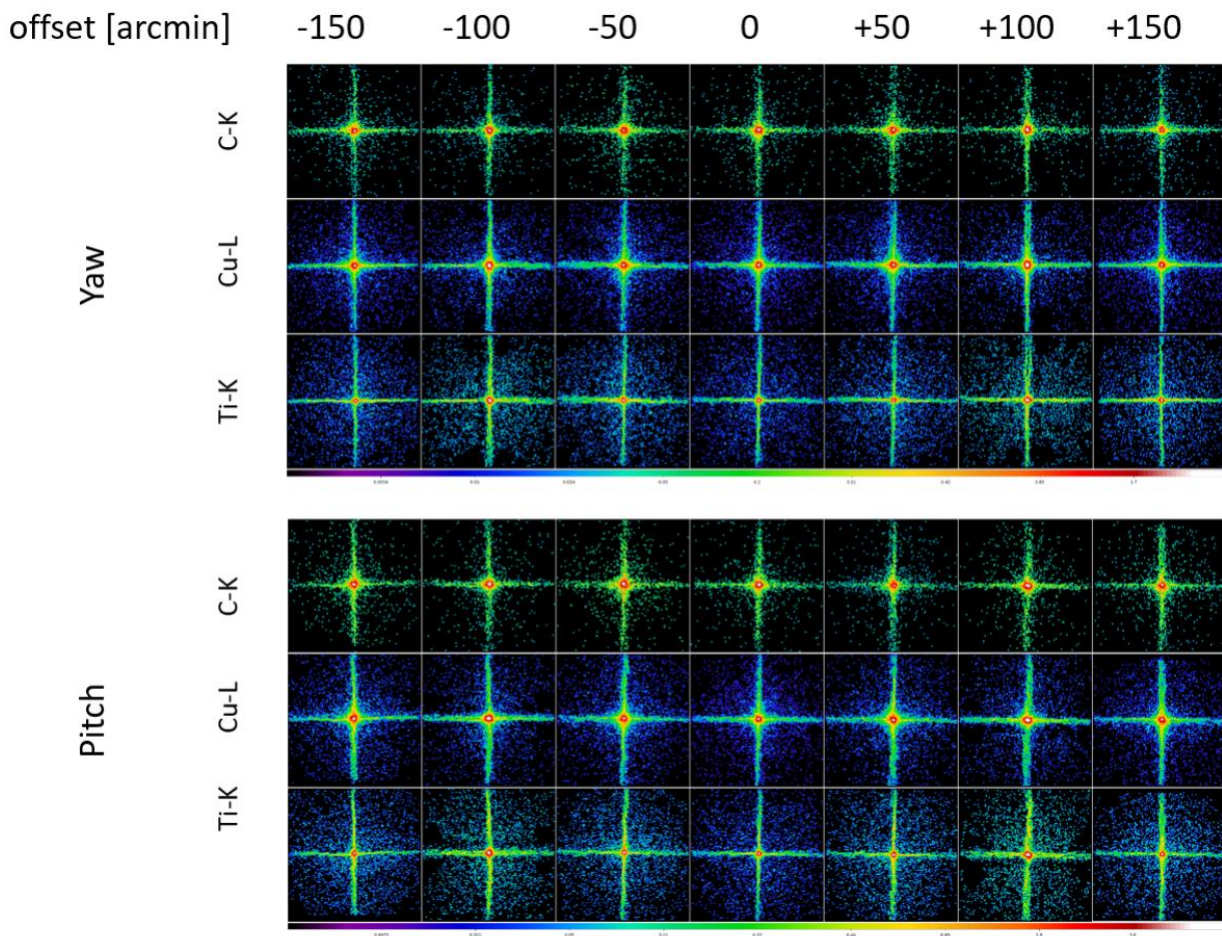


Figure 28 Compilation of PSF exposures for the focal plane mapping at sector 2 in horizontal (yaw), vertical (pitch) direction at C-K, Cu-L and Ti-K for the off-axis angle from -150 arcmin to 150 arcmin

Effective Area

The effective area measurements were carried out at very low Energy band continuum (vIEbc) and low Energy band continuum (lEbc) for the single reflection, double reflection, and direct beam for all sectors. The results match well with the theoretical model from the EP team. For the vIEbc (500 - 2000 eV), the embedded lines used for the effective area calculation are O-K (525 eV) and Al-K (1490 eV). While for the lEbc (700-4000 eV), the embedded lines are Ti-L (452 eV) and W-M (1780 eV). Figure 29 shows the measurement results of the effective area at the vIEbc and lEbc overlay with the model from the EP team (Chen Model) and UoL team (Dick Model). The data points from single energy measurements are also included in the plot.

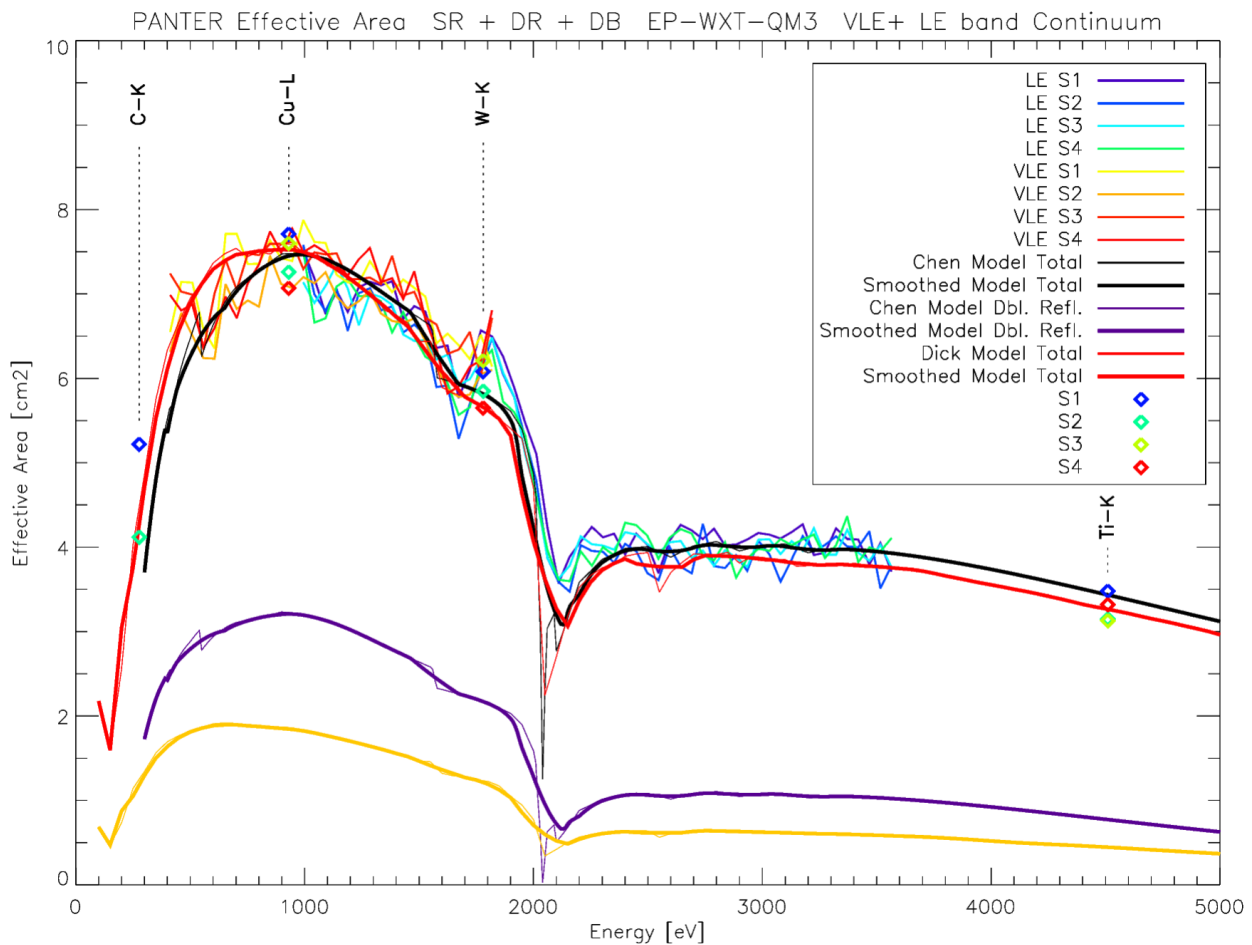


Figure 29 The effective area of single reflection, double reflection, and direct beam at vLEbc (VLE) and lEbc(LE) for all 4 sectors (S1, S2, S3, S4) in comparison with different models

4.4.4 DISCUSSION EP-WXT

The Einstein Probe WXT QM was tested at PANTER at the energies: very low Energy band continuum (vLEbc), low Energy band continuum (lEbc) Cu-L, Ti-K, and C-K. The mirror module has undergone measurements under X-ray. Since the TRoPIC detector is set to be perpendicular to the optical axis, not at the focal plane of each sector, additional movement was required for the optic and detector to align each sector. The mirror sector was rotated by range $\pm 5.4^\circ$ in pitch and yaw with respect to the optical axis. The detector was translated in Pantolsky-Wald or Up-Down direction by 71 mm for the measurement. As a result, this introduced an additional shift of 9.5 mm along the optical axis. During the alignment under X-ray, we have noticed a slight plate misalignment at the lower right corner (sector 4) of the Figure 22 that was not well aligned with the other sectors in comparison to the simulation. However after the focus searches for all sectors, the average FWHM for all sectors was ~ 4.1 arcmin from the PANTER analysis. We have analysed the PANTER best focus with independent analysis to those of UoL on the same dataset. The best focus position for all but one sector (4) differed by less than 0.5 mm. Sector 4 was measured to have the shortest focal length among all the sectors.

After the focal length of each sector was measured, the on-axis extended mosaic PSF was characterized. The PSF at different energies confirms that the mirrors are more sensitive (collect more X-ray photons) towards the vIEbc and Cu-L – see results in Figure 24 and Figure 26, compared to ones taken at Ti-K in Figure 25. A ‘map’ of the focal plane of the MOP depending on the off-axis angle was created at C-K, Ti-K and Cu-L. The resulting PSFs in their corresponding positions are displayed in a single image for each energy. The full mapping of all sectors was carried out at Cu-L including the off-axis angle ranging ± 150 arcmin shown in Figure 28. Our results show that sector 1 has the best alignment among all the MPO chips within that sector. Sector 2 and 4 has slight separation of the single reflection, from mis-alignment of the MPOs, at the far end (± 150 arcmin) of the off-axis focal plane. Sector 3 shows a similar effect especially at the off-axis angle -50 to -150 arcmin. The characterization of the mapping only the horizontal (yaw), and vertical (pitch) at different energies shows an effect of X-ray scattering towards the higher energy. It creates ‘halo’ around the double reflection spot, clearly shown in the images taken at Ti-K. This could be caused by the micro roughness on the mirror surface. Lastly, the effective area measurement of vIEbc and IEbc combination for all sectors agrees well with the theoretical model – see Figure 29. The number is also proportional to the quality of the alignment within each sector.

The development of the WXT mirror module has currently gone to the flight model (FM) phase. PANTER is expecting the next characterization of a WXT FM optic in Fall 2022.

4.5 ATHENA: Testing a SPO Calibration Reference Mandrel

The objective of the measurement campaign was to determine the performance of the optic, specifically the half-energy width (HEW) at 1.49 keV (Al-K). This optic is to serve as the optical ‘standard’ to compare the x-ray measurement capabilities of different facilities, in preparation for the ATHENA mirror construction and testing.

4.5.1 THE OPTIC

The optic was built by cosine measurement systems, and is identified as XOU-0055 (MM-0037). XOU-0055 is a single-shell system, comprising two mandrels produced by Zeiss – one characterised to represent the primary mirror and the other the secondary mirror. Together the two mandrels form a single reflecting ‘layer’ of the x-ray optic unit (XOU). General information on the manufacturing and construction of silicon pore optics can be found elsewhere [17, 18] XOU-0055 was mounted inside a mirror module (MM) structure for testing at PANTER. A dummy block was placed in the second XOU position of the MM, to give the necessary mechanical stiffness to the optic structure. The dummy block did not contribute to the measurement results.

Table 7 gives the specifications of the optic. Figure 30 shows a photograph of the optic prior to installation at the PANTER facility.

Table 7 Specifications of the XOU-0055 optic, comprising two mandrels to create one silicon reflective ‘layer’

| Parameter | Value |
|----------------------------------|------------------|
| MM name | MM-0037 |
| XOU name | XOU-0055 |
| Number of silicon pore layers | 1 |
| Radius of curvature | 737 mm |
| Focal length (nominal) | 12000 mm |
| Focal length (measured at BESSY) | 11975 mm |
| Separation between mandrels | 0.5 ± 0.2 mm |

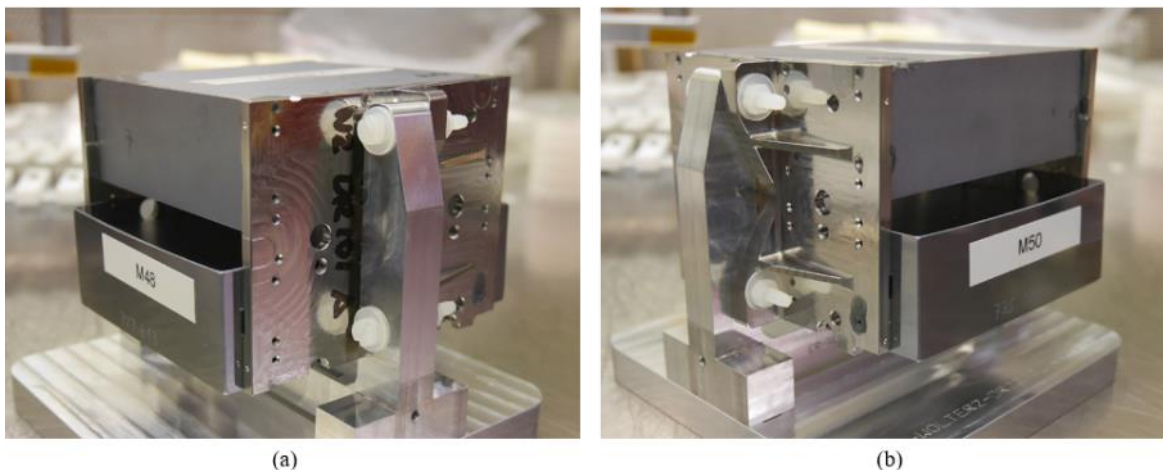


Figure 30 Photograph of the XOU-0055 mandrel optic, showing (a) the parabolic M48 mandrel and (b) the hyperbolic M50 mandrel (Photo credit: cosine measurement systems)

4.5.2 TEST METHODOLOGY

The test method for this optic followed the same method as previous ATHENA MM test campaigns at PANTER [19, 20]. As such, only a brief description is given here.

Installation and Setup

The optic was installed on its side, as the ~ 12 m focal length of the optic restricted the setup to certain configurations. Figure 31a shows the optic installed in the PANTER chamber attached to a hexapod, which allows fine movements of the optic once under vacuum. The pivot point of the hexapod is set to the centre of the optic. To assist the reader in visualising the measurements in this paper, the ‘top’ of the optic is the edge of the optic closest to the roof of the facility, and the ‘bottom’ of the optic is closest to the ground. A moveable mask was installed between the optic and x-ray source, with apertures capable of illuminating 100%, 48%, and 4% of the optic. These

apertures were chosen to enable characterisation of the full optic and of specific sections of the optic. The mask is visible in Figure 31a.

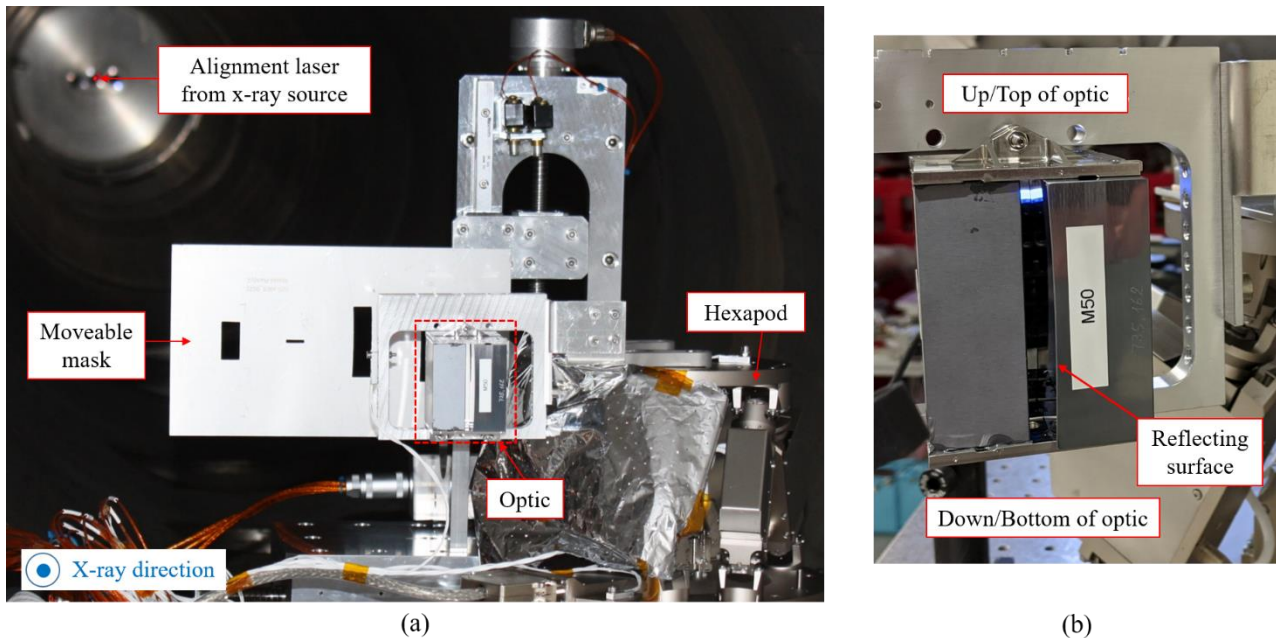


Figure 31 (a) The XOU-0055 mounted inside the PANTER chamber attached to a hexapod, to enable fine adjustment of the optic under vacuum. The moveable mask used to illuminate either the full optic or a chosen section of the optic is also shown. The MLI between the optic and the hexapod protects the optic from the heat produced by the hexapod motors. (b) The optic in its holding structure at the PANTER facility, showing the nomenclature for the measurements of the optic during this campaign. (Credit: MPE)

Alignment

Once under x-ray illumination, the 100% mask was aligned over the optic by observing the total x-ray count rate for the optic. The mask was moved incrementally and the corresponding change in count rate was observed using the online detector tool. Once the 100% mask was aligned, the 4% mask was aligned using geometric distances from the mask CAD drawing, then finely adjusted by eye to observe when the x-ray scattering around the point spread function (PSF) was and was not visible.

The optic was aligned in pitch and yaw using the 100% mask. This is part of the standard optical alignment method at PANTER, the aim of which is to minimise the HEW and maximise the flux over a range of pitch and yaw angles [19].

Once the optic alignment in pitch and yaw was completed, a focus search [19] was carried out to determine the best focus position for the detector. The detector was translated towards and away from the x-ray source ± 50 mm around the initial in-chamber alignment position in steps of 5 mm. An exposure was made at each of these positions, and the corresponding HEW, x-FWHM, and y-FWHM calculated. Fitting a parabola to the data determined the minimum HEW and y-

FWHM and the corresponding 'best focus' position. The γ -FWHM was taken as the final fitting metric, due to the variance of the HEW across the optic surface.

Cosine had measured the optic at BESSY, at the PTB XPBF 2.0 beamline [20], prior to this campaign. As such, it was known that the best focus position varied across the optic. It was decided that a second focus search should be carried out, for the bottom half of the optic, using the 48% mask, where the best HEW performance was expected. The bottom-of-optic best focus position deviated from the complete optic best focus position by 28.7 mm.

4.5.3 Measurements

All measurements were made at Al-K (1.49 keV).

Single-Exposure PSF (HEW)

Single-exposure PSF images were made at the position of best focus for the full optic, using the 100% mask, for approximately 10,000 counts. These exposures were used as preliminary HEW measurements.

Azimuthal Scan (HEW)

An azimuthal scan was carried out using the 4% mask in the best focus position for the full optic. This type of scan allows closer analysis of the optic surface, as the 4% mask illuminates only 2.5 mm of the optic per exposure. A total of 24 exposures were made, starting from the top of the optic and covering the full length of the optic.

Pixel Scan (HEW)

Following the single PSF images and the azimuthal scan, two pixel scans^{3,5} were made: one for the full optic and one for the bottom of the optic. A pixel scan increases the measurement resolution of the HEW by enabling sub-pixel resolution; the detector pixels are 0.075 mm x 0.075 mm, and with a 6x6-exposure pixel scan the detector movement pitch is 0.0125 mm. This measurement scans over the pixel, and is necessary because the PSF of this optic is so small that the photons encircled in the "HEW circle" during the analysis are mainly detected in one pixel. Each full pixel scan (36 exposures) yields one HEW value.

Intra-Focal/Extra-Focal Images

Intra-focal and extra-focal images were made of the optic, to expose any features that were not visible in the focused PSF images. Two extra-focal images and one intra-focal image were taken of the full optic using the 100% mask. These were made 340 mm and 250 mm extra-focal, and 220 mm intra-focal from the full optic best focus position. One extra-focal image was taken of the bottom of the optic using the 48% mask. This was taken 340 mm extra-focal from the bottom-of-optic best focus position.

4.5.4 RESULTS

The key results of the campaign are presented in this section, separated into the HEW (the key performance indicator) and the intra-focal and extra-focal images.

HEW

Table 8 presents the HEW values measured during this campaign using both single exposures and pixel scans. The pixel scan method is more precise thus it was expected that it would yield a slightly different HEW value to that of the single exposure method. Figure 32 shows the resulting PSF for the two pixel scan measurements.

Figure 33 shows the plot of all 24 azimuthal scan HEW values for the full optic. The azimuthal measurements were made prior to the pixel scans, thus it was possible to identify the region of lowest HEW – the bottom ~30% of the optic. It is believed that the HEW of the optics varies in the sagittal direction due to the meridional curvature of the optics varying across the sagittal direction. Why this occurs is ongoing, but the measurements taken at cosine are compatible with this probable cause.

Table 8 The HEW values of the optic for each measurement set, showing the mask used and the section of the optic imaged

| Mask (%) | Section of Optic | Method | HEW (arcsec) |
|----------|------------------|-----------------|--------------|
| 100 | Full | Single exposure | 2.7 |
| 100 | Full | Pixel scan | 2.9 ± 0.1 |
| 48 | Bottom (~30%) | Pixel scan | 2.2 ± 0.1 |

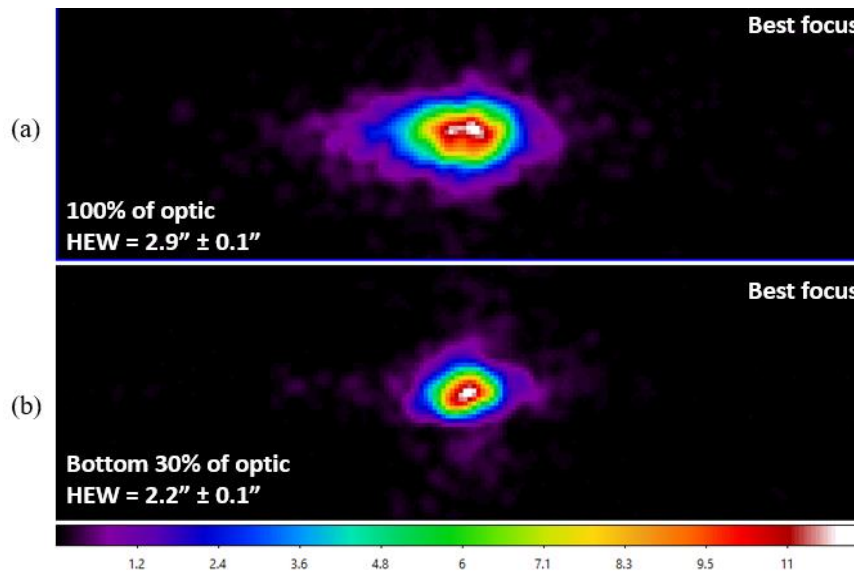


Figure 32 The best focus PSF image for (a) the full optic with the 100% mask, and (b) the bottom ~30% of the optic with the 48% mask. The corresponding HEW values are written on the appropriate image. (Credit: MPE)

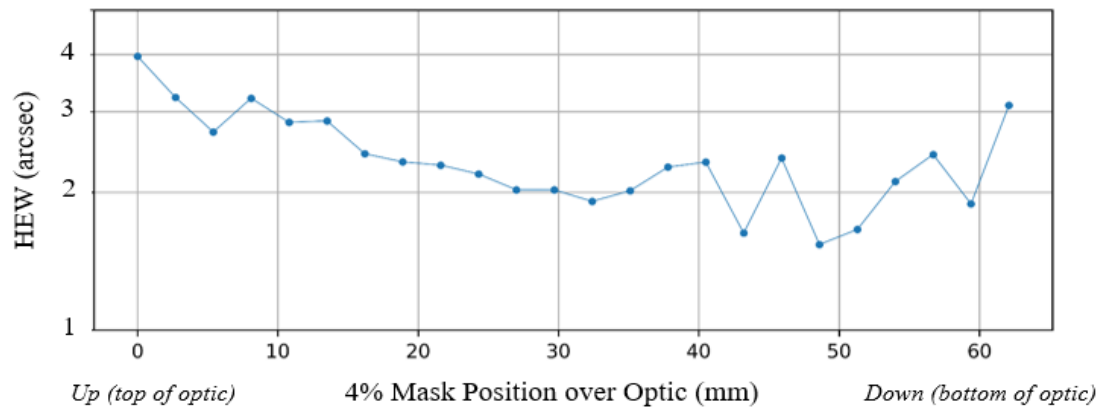


Figure 33 The HEW at each position of the azimuthal scan, aligning the 4% mask in front of the optic, starting at the ‘top’ of the optic, and measuring 24 separate positions (each one a separate exposure) to the ‘bottom’ of the optic. (Credit: MPE)

Intra-Focal/Extra-Focal Images

Figure 34 shows the intra-focal (220 mm) image for the full optic, using the 100% mask. Figure 35 shows the extra-focal at 250 mm and Figure 36 the extra-focal image at 340 mm for the full optic, using the 100% mask. It is clear in the distortion of the images that there is a difference across the reflecting surface of the optic. However, no unexpected features were observed in the images.

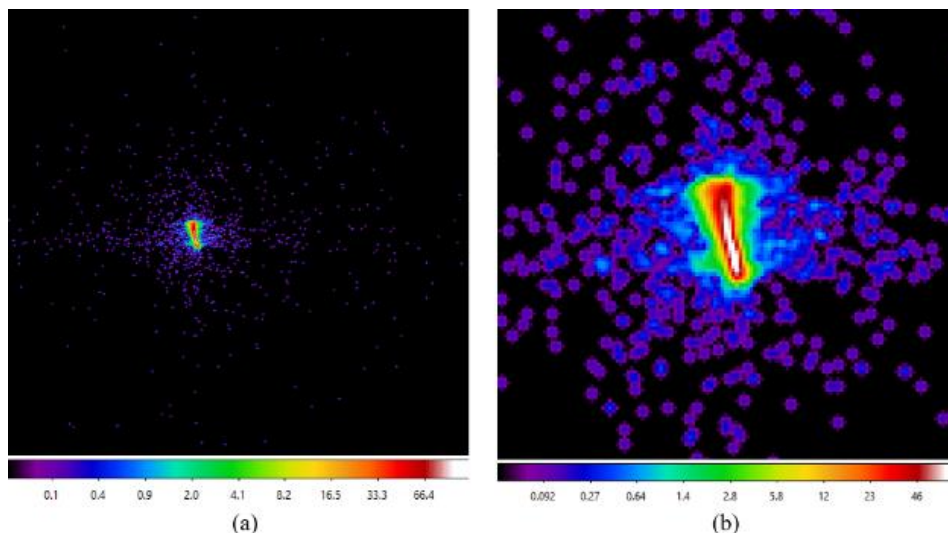


Figure 34 Intra-focal 220 mm (a) full image and (b) x4 zoomed image of XOU-0055, at the best full optic focus position, taken at Al-K using the 100% mask.

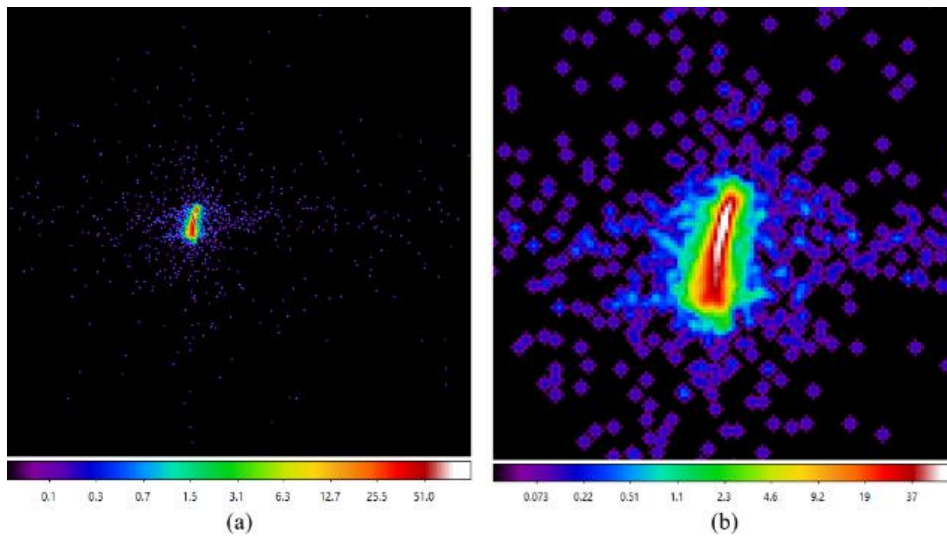


Figure 35 Extra-focal 250 mm (a) full image and (b) x4 zoomed image of XOU-0055, at the best full optic focus position, taken at Al-K using the 100% mask.

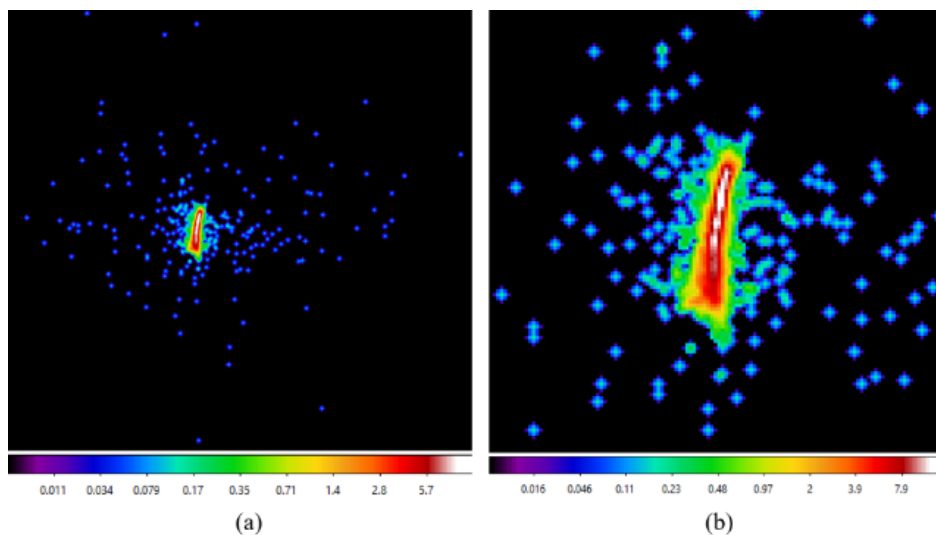


Figure 36 Extra-focal 340 mm (a) full image and (b) x4 zoomed image of XOU-0055, at the best full optic focus position, taken at Al-K using the 100% mask.

4.5.5 SUMMARY

The XOU-0055 mandrel optic has a global performance of $2.9 \text{ arcsec} \pm 0.1 \text{ arcsec}$ (HEW at 1.49 keV). Despite a non-symmetric optical surface, no unexpected deviations across the surface of the optic were observed. This optic can be used to measure the performance of other x-ray integration and test facilities designed for ATHENA SPOs.

4.6 Other Campaigns at PANTER

4.6.1 X-ray Optics for BEaTriX

The high precision X-ray optics needed for the BEaTriX test facility at INAF/Brera needed to be calibrated. BEaTriX is also supported a this AHEAD2020 X-ray optics JRA and details are given in the AHEAD2020 WP10 deliverables D61 [22] and D64 [23]. To test this optic it is was important to have a parallel X-ray beam at PANTER for which an extra campaign was set up. This parallel X-ray beam was developed at and for PANTER supported by the original AHEAD grant. It consists of a Fresnel Zone Plate with a focal length of 120 meter at Al-K (1.49 keV) that generates a 40 mm x 60 mm large parallel X-ray beam that can fully illuminate the high precision parabola for BEaTriX. The parabola was tested uncoated and after gold coating in DTU. Figure 37 shows the parabola mounted in PANTER and the measured PSFs.

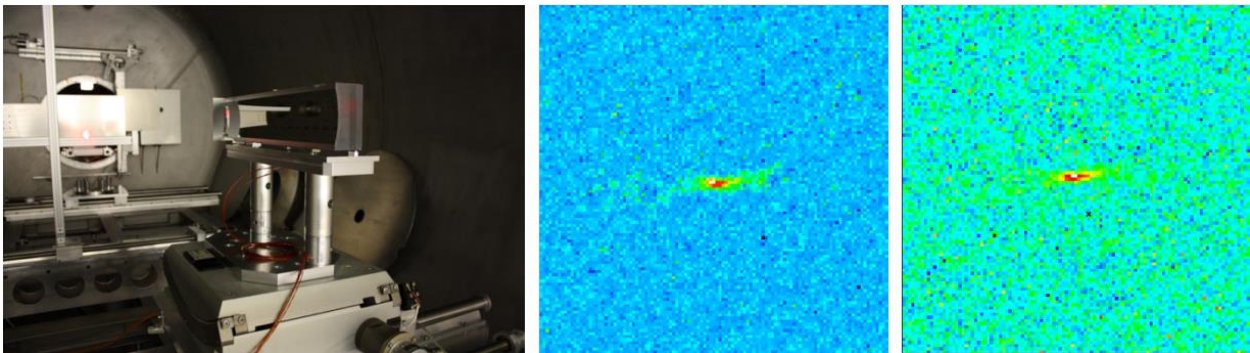


Figure 37 (left) the BEaTriX paraboloidal mirror mounted in PANTER, viewed from the detectors side. (center) Best focus measured with PIXI at 1.49 keV in parallel setup, before coating, HEW = 3.1 arcsec. (right) Same as previous image but after coating, HEW = 2.8 arcsec.

4.6.2 Lobster-eye and K-P Baez optics

As part of the AHEAD2020 X-ray optics JRA several Lobster-Eye and K-P Baez optics were studied at PANTER. The results from these tests have been very useful and they are being used to improve many aspects in the design, production and X-ray testing of the optics. The results of these tests will be reported on in upcoming AHEAD2020 deliverables (see Figure 38).

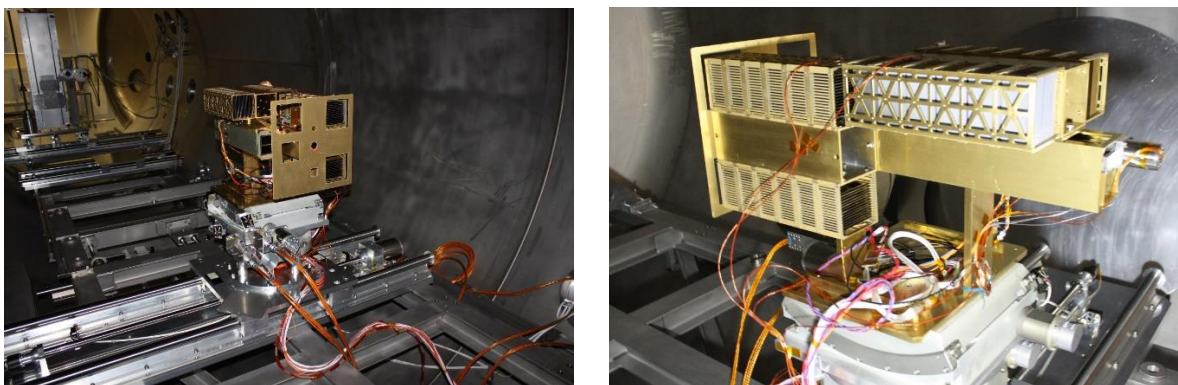


Figure 38 Large KB module at the PANTER facility. (left) view from X-ray source, (right) the side view.

5 Summary

About 30 test campaigns took place at MPEs PANTER X-ray test Facility in the period March 2020 to January 2022. Most of the campaigns were in part supported by the AHEAD2020 “X-ray optics” joint research activity.

The majority of these campaigns was performed to characterise the quality of the optics that have been developed for the approved missions SVOM and Einstein Probe. These missions are Chinese – European collaborations see Sections 4.1, 4.2, 4.3, and 4.4. For SVOM all FM optic and telescope activities and for Einstein-Probe all the QM activities were successfully completed.

As the ATHENA silicon pore optics production came to a stop due to the closure of BESSY in Berlin, to outside groups for a long period of time due to Covid19 only optics that were available at the time were used for tests.

- The detailed measurement of calibration reference mandrel optic is discussed in detail in Section 4.5. This optic will be used to test the quality and precision of measurement of the different X-ray test facilities involved in the production and characterisation of the silicon pore optics.
- The time was used also to test the effects of particle contamination on the effective area of the SPOs using an already available optic at PANTER. This was done by exposing a SPO MM-0036 to 1000 ppm and 2000 ppm total particle contamination. The main result from these tests is that the no measurable change in effective area is detected.
- The high precision collimating parabola for BEaTriX was successfully tested at PANTER using the PANTER parallel X-ray Beam generated using a specially designed Fresnel-Zone-Plate.

Many campaigns to test and characterise lobster-eye and K-P Baez type optics were performed. The results from these tests have been very useful and they are being used to improve many aspects in the design, production and X-ray testing of the optics.

The PANTER X-ray test facility ran continuously the Covid19 pandemic and found new ways to perform measurements where the optics creators where not able to join the measurement campaigns in person. Now gradually these activities are returning to normal testing routines with the teams responsible for the optics joining the measurements in person.

Bibliography

- [1] Gonzalez, F. and Yu, S. 2018, "SVOM: a French/Chinese cooperation for a GRB mission", Proc. SPIE 10699, Space Telescopes and Instrumentation 2018: Ultraviolet to Gamma Ray, 1069920, doi: 10.1117/12.2311710
 - [2] Mercier, K., Gonzalez, F., Götz, D., et al. 2018, "MXT instrument on-board the French-Chinese SVOM mission," Proc. SPIE 10699, Space Telescopes and Instrumentation 2018: Ultraviolet to Gamma Ray, 1069921, doi:10.1117/12.2313561
 - [3] Willingale, R., Pearson, J.F., Martindale, A, et al. 2016, "Aberrations in square pore micro-channel optics used for x-ray lobster eye telescopes," Proc. SPIE 9905, Space Telescopes and Instrumentation 2016: Ultraviolet to Gamma Ray, 99051Y, doi:10.1117/12.2232946
 - [4] Meidinger, N., Andritschke, R., Hälker, O., et al. 2006, Nuclear Instruments and Methods in Physics Research A, 568, 141, doi: 10.1016/j.nima.2006.05.268
 - [5] Meuris, A., Pinsard, F., Doumayrou, E., et al.2014 "The camera of the Microchannel X-ray telescope onboard the SVOM mission," Proc. SPIE 9144, Space Telescopes and Instrumentation 2014: Ultraviolet to Gamma Ray, 91444Z (24 July 2014); doi:/10.1117/12.2055162
 - [6] Yuan, W., Zhang, C., Feng, H., Zhang, S. N., Ling, Z. X., Zhao, D., Deng, J., Qiu, Y., Osborne, J. P., O'Brien, P., Willingale, R., Lapington, J., Fraser, G. W., and the Einstein Probe team, 2015 "Einstein Probe – a small mission to monitor and explore the dynamic X-ray Universe," arXiv e-prints , arXiv:1506.07735
 - [7] Yuan, W., Zhang, C., Ling, Z., Zhao, D., Wang, W., Chen, Y., Lu, F., Zhang, S.-N., and Cui, W, 2018 "Einstein Probe: a lobster-eye telescope for monitoring the x-ray sky", Proc. SPIE 10699, Space Telescopes and Instrumentation 2018: Ultraviolet to Gamma Ray, 1069925, doi:10.1117/12.2313358
 - [8] Feldman, C., O'Brien, P., Willingale, R., Zhang, C., Ling, Z., Yuan, W., Jia, Z., Jin, G., Li, L., Xu, Z., Zhang, Z., Lerman, H., Hutchinson, I., McHugh, M., and Lodge, A., 2020 "Testing of the WXT optics at the University of Leicester", Proc. SPIE 11444, Space Telescopes and Instrumentation 2020: Ultraviolet to Gamma Ray, 114447R, doi:10.1117/12.2562194
 - [9] Chen, Y., et al. 2020, "Status of the follow-up X-ray telescope onboard the Einstein Probe satellite", Proc. SPIE 11444, Space Telescopes and Instrumentation 2020: Ultraviolet to Gamma Ray, 114445B, doi:10.1117/12.2562311
 - [10] Predehl, et al., 2021 "The eROSITA X-ray telescope on SRG," A&A 647, A1, doi:10.1051/0004-6361/202039313
 - [11] Bradshaw, M., Burwitz, V., Friedrich, P., Hartner, G., Langmeier, A., Valsecchi, G., Vernani, D., and Chen, Y., 2020, "X-ray testing of the Einstein Probe follow-up X-ray telescope STM at MPE's PANTER facility", Proc. SPIE 11444, Space Telescopes and Instrumentation 2020: Ultraviolet to Gamma Ray, 1144457, doi:10.1117/12.2560972
 - [12] Feldman, C., 2021, "Einstein Probe QM module tests at PANTER (tn18 for wp 1.4)," techreport Issue 1 Rev:2, University of Leicester.
-

-
- [13] Barret D., et al., 2020, "The Athena space X-ray Observatory and the astrophysics of hot plasma", *Astronomische Nachrichten / Astronomical Notes (AN)*, 341 (2), doi:10.1002/asna.202023782
 - [14] Barret, D. et al., 2018 "The ATHENA X-ray Integral Field Unit (X-IFU)", *Proc. SPIE 10699, Space Telescopes and Instrumentation 2018: Ultraviolet to Gamma Ray*, 106991G, doi:10.1117/12.2312409
 - [15] Meidinger N., et al., 2020, "Development status of the wide field imager instrument for Athena", *Proc. SPIE 11444, Space Telescopes and Instrumentation 2020: Ultraviolet to Gamma Ray*, 114440T, doi:10.1117/12.2560507
 - [16] Bavdaz M., et al., 2021, "The Athena x-ray optics development and accommodation", *Proc. SPIE 11852, International Conference on Space Optics — ICSO 2020*, 1185220, doi:10.1117/12.2599341
 - [17] Collon, M. et al., 2019, "Status of the silicon pore optics technology", *Proc. SPIE 11119, Optics for EUV, X-Ray, and Gamma-Ray Astronomy IX*, 111190L, doi:10.1117/12.2530696
 - [18] Landgraf B. et al., 2019, "Development and manufacturing of SPO X-ray mirrors", *Proc. SPIE 11119, Optics for EUV, X-Ray, and Gamma-Ray Astronomy IX*; 111190E, doi:10.1117/12.2530941
 - [19] Bradshaw M. et al., 2019, "Developments in testing x-ray optics at MPE's PANTER facility", *Proc. SPIE 11119, 11119-16*, doi:10.1117/12.2531709
 - [20] Burwitz V. et al., 2018, "X-ray testing at PANTER of optics for the ATHENA and Arcus Missions", *Proc. SPIE 11180, 1118024*, doi:10.1117/12.2535995
 - [21] Handick E. et al., 2020, "Upgrade of the x-ray parallel beam facility XPBF 2.0 for characterization of silicon pore optics", *Proc. SPIE 11444, 114444G*, doi:10.1117/12.2561236
 - [22] AHEAD2020 WP10 deliverable D10.1-D61 (2021) "Report on beam conditioning optics for test facilities".
 - [23] AHEAD2020 WP10 deliverable D10.4-D64 (2022) "Advancement on the new high-precision metrology systems for testing X-ray optics".